

Marshall University

Marshall Digital Scholar

Theses, Dissertations and Capstones

2022

Sequential assembly of 1-D and 2-D origami arrays

Nathan Shin

Follow this and additional works at: <https://mds.marshall.edu/etd>



Part of the [Analytical Chemistry Commons](#), and the [Physical Chemistry Commons](#)

SEQUENTIAL ASSEMBLY OF 1-D AND 2-D ORIGAMI ARRAYS

A thesis submitted to
Marshall University
in partial fulfillment of
the requirements for the degree of
Master of Science
in

Chemistry

by

Nathan Shin

Approved by

Dr. Michael Norton, Committee Chairperson

Dr. Scott Day

Dr. Rosalynn Quinones-Fernandez

Marshall University

May 2023

Approval of Thesis/Dissertation

We, the faculty supervising the work of Nathan Shin, affirm that the thesis, *Sequential Assembly Of 1-D And 2-D Origami Arrays*, meets the high academic standards for original scholarship and creative work established by the Chemistry Department and the Graduate College of Marshall University. The work also conforms to the requirements and formatting guidelines of Marshall University. With our signatures, we approve the manuscript for publication.



Dr. Michael Norton, Department of
Chemistry

Committee Chairperson

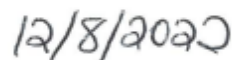


Date



Dr. Scott Day, Department of Chemistry

Committee Member



Date



Dr. Rosalynn Quinones-Fernandez,
Department of
Chemistry

Committee Member



Date

© 2023
Nathan Shin
ALL RIGHTS RESERVED

ACKNOWLEDGMENTS

I want to thank all the people who helped me along the way. Dr. Norton, David Neff, Mom, and Dad, Thank you for your support.

TABLE OF CONTENTS

List of Tables	viii
List of Figures	ix
Abstract	xii
Chapter 1 INTRODUCTION.....	1
DNA Origami.....	3
Biotin Binding to Streptavidin.....	4
Superresolution Microscopy	5
Characterizing Plasmon Spectra for Assemblies	8
CHAPTER 2 PROPOSED APPROACH AND DESIGN	10
CHAPTER 3 0-D and 1-D ARRAYS.....	13
CO-01.....	13
CO-3970.....	15
Types of Origami Junctions	17
Infinite vs Finite 1-D Arrays.....	19
Parallel vs Rotated 1-D Arrays	23
Alternating vs Homogeneous 1-D Arrays.....	23
CHAPTER 4 2-D ARRAYS.....	25
Infinite vs Finite 2-D Arrays.....	25
Parallel vs Rotational 2-D Arrays	26
Homogeneous vs Alternating 2-D Arrays.....	26
CHAPTER 5 MODIFICATION SITES	28
Biotin and Streptavidin	28

Molecular Beacon (MBv2)	31
Gold Nanoparticle (AuNP) with Dendrimer.....	31
CHAPTER 6 METHODS.....	32
CO Monomer Synthesis	33
NanoDrop Analysis.....	34
Mica Substrate Preparation	34
Mica Substrate Deposition	35
AFM Imaging.....	36
Streptavidin (SA) Decoration.....	38
Thermal Anneal Programs and Time Variations for 1-D Array Growth.....	38
Diafiltration.....	39
Gel Electrophoresis	40
Gel Analysis	41
On-Mica Deposition.....	42
On-Glass Deposition	42
Refined Dendron to Conjugated DNA Synthesis	43
CHAPTER 7 RESULTS AND DISCUSSION.....	48
Thermal Anneals	48
3 Base Pair (BP) Sticky Ends (SE) vs 5 BP SE	52
Nucleated Growth and Successive Addition.....	55
Gel Purification	58
On Mica Assembly	60
On Glass Assembly	62

Dendrimer and Gold Nanoparticle	63
CHAPTER 8 CONCLUSION.....	68
References.....	70
APPENDIX A: OFFICE OF RESEARCH INTEGRITY APPROVAL LETTER.....	74
APPENDIX B: LIST OF ABBREVIATIONS	75
APPENDIX C: FIGURE PERMISSION FOR SEEMAN’S CO-01 DESIGN	77
APPENDIX D: S1 AND S6.....	78
APPENDIX E: Monomer Count for Table 3	79

LIST OF TABLES

Table 1	Reagent List for CO-01 0-D with Modified Sites for Biotin.	33
Table 2	Loading Lanes for Gels.	41
Table 3	Monomer Count for Each Variation in Stoichiometric Experiments.	55
Table 4	Entry Association with Experiments in Figure 43.	66
Table 5	S1 Contents	78
Table 6	S6 Contents	78

LIST OF FIGURES

Figure 1	Self-Assembly of DNA Origami.	1
Figure 2	Fast Scan AFM and Fluorescence Microscope.	5
Figure 3	Förster Resonance Energy Transfer.	7
Figure 4	G2 PAMAM Dendrimer.	8
Figure 5	Modular parts of the Refined Dendron to Conjugated DNA with a Long Tether. ...	9
Figure 6	Legend of Illustrated CO.	10
Figure 7	Design of Alternating 1-D Linear Array of CO-01 and CO-3970 with MBv2 on the Left Arm of each CO-01.	11
Figure 8	Dendron to Conjugated DNA.	12
Figure 9	CO Map of CO-01.	14
Figure 10	CO Map of CO-3970.	16
Figure 11	3 BP SE Overhang vs 5 BP SE Overhang.	18
Figure 12	AFM Image of “Infinite” 1-D Arrays.	20
Figure 13	Infinite vs Finite 1-D Arrays.	21
Figure 14	Finite 1-D Array.	22
Figure 15	Parallel vs Rotated 1-D Arrays.	23
Figure 16	Homogeneous vs Alternating 1-D Arrays.	24
Figure 17	Infinite vs Finite 2-D Arrays.	25
Figure 18	Parallel vs Rotational 2-D Arrays.	26
Figure 19	Homogeneous vs Alternating 2-D Arrays.	27
Figure 20	CO-01 with Streptavidin Labeling on the Left and Right Arms.	28
Figure 21	Helical Structure of DNA.	29

Figure 22	Biotin Modified Staple Sites on CO-01.....	30
Figure 23	Design of MBv2 Implemented into CO-01.....	31
Figure 24	Design of Gold Nanoparticle and Dendron into CO-01.....	32
Figure 25	Mica Substrate.	35
Figure 26	Simple Humidity Chamber.	36
Figure 27	Bruker Multimode 8 and Cantilever.	37
Figure 28	Nucleated Growth Through Titration.....	39
Figure 29	Protocol for Synthesized Conjugates.....	44
Figure 30	Thermal Anneal Program Comparison	48
Figure 31	CO-01 T and CO-3970 with SA	50
Figure 32	CO-01 with MBv2 and CO-3970 with Thermal Program of 45°C to 6°C for 24 Hours.....	51
Figure 33	3 BP SE vs 5 BP SE.....	52
Figure 34	Stoichiometric Experiments.	53
Figure 35	Nucleated Growth Through Successive Addition.....	56
Figure 36	Diafiltered Nucleated Growth Through Successive Addition	57
Figure 37	Gel Image of 3 Different Stains Using Dimer Sample.	58
Figure 38	Shadowing Technique Using Dimer Sample.....	59
Figure 39	UV-Table Guided Extraction Using Dimer Product.....	60
Figure 40	On Mica Assembly of 2-D Arrays.....	61
Figure 41	On Glass Assembly of 2-D Arrays.	62
Figure 42	Gel with Refined Dendron to Conjugated DNA.....	64

Figure 43	Shows the Color Shift of AuNP Solution when Adding Different Types of Salts and Refined Dendron to Conjugated DNA.	65
Figure 44 A	4:1 CO-01 to CO-3970.	79
Figure 44 B	2:1 CO-01 to CO-3970.	80
Figure 44 C	1:1 CO-01 to CO-3970.	80
Figure 44 D	1:2 CO-01 to CO-3970.	81
Figure 44 E	1:4 CO-01 to CO-3970.	82

ABSTRACT

DNA origami, invented by Paul Rothemund in 2006, provides many possible routes for the synthesis of complex macromolecular assemblies. This project involves the creation of 1-D and 2-D arrays of cross origami to support the development of DNA detection devices by providing precise platforms for these devices. The M13 plasmid is the most commonly used scaffold in DNA nanotechnology, limiting the size and complexity of an individual DNA origami construct. However, by creating larger assemblies, the dimensions can be multiplied. For example, by alternating two different types of cross origami, optical reporters can be separated by 200 nm, which is beyond the Abbe optical limit for optical microscopy. Due to apparent low yields of longer alternating structures and high amounts of shorter by-products, the research was directed into creating and purifying dimers to be utilized as “building blocks” for arrays. With dimers being utilized as the new “building blocks”, several different designs were created to expand the support systems for optical imaging. Two approaches were primarily utilized. The first approach is the assembly of 1-D arrays of origami dimers. The idea of generating and purifying dimers as the new “building block” was to simplify the process by maintaining a 1:1 stoichiometry of the two-component origami structure; however, a low yield of the new “building block” at the purification/isolation stage redirected the research to the second approach. The second approach consisted of a multi-step assembly approach which eliminated the dimer isolation stage and allowed the production of much more favorable yields. A primary 1-D array of controlled length was generated by using a fixed stoichiometry of chain termination constructs to monomer components. A second 1-D row array was then assembled on this primary array. This in turn led to the creation of an array of dimers. The final step in creating the 2-D array was to cross-link the DNA origami in the second row. After extensive research, it

was observed that there was a limitation with on-surface immobilized dimer cross linking using mica as the substrate. Since glass is the desired final substrate for sample deposition, finding a technique to give a better population of arrays per unit area was necessary. Thus, in solution reaction on glass was employed to allow for inter-strand cross linking to create dimer arrays for the assembly of sensing device platforms.

CHAPTER 1

INTRODUCTION

DNA nanotechnology is a branch of nanotechnology taking advantage of the physical and chemical properties of DNA to design, study, and apply it as a synthetic structure. The DNA origami structures described here have evolved from Rothemund's original design¹ to Seeman's design² of the cross origami (CO) to Tsai Chin Wu's assembly of finite and infinite 1-D arrays.³ DNA origami, specifically our cross origami, is composed of a single stranded viral DNA sequence (M13), known as a scaffold strand, and approximately 200 synthetic oligonucleotides averaging 32 bases in length, known as the staple sequences. These staple sequences are designed to be complementary to multiple sites on the scaffold and direct self-assembly and folding of the scaffold into two orthogonal rectangles that come together to form a cross shown in Figure 1.

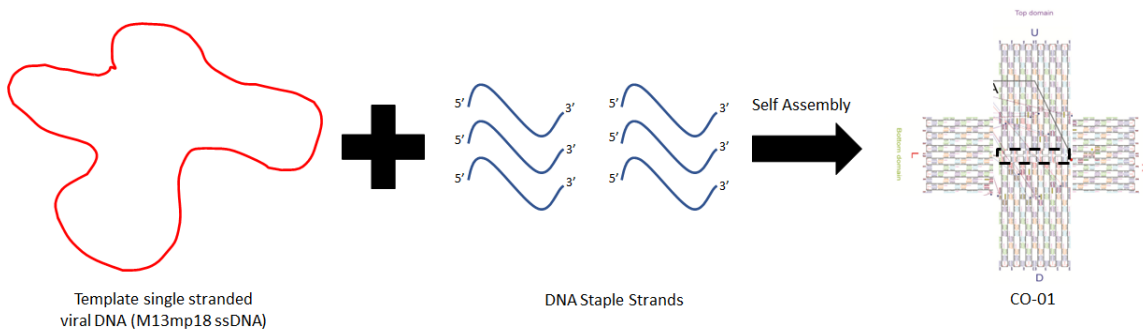


Figure 1. Self-Assembly of DNA Origami. Depiction of a single stranded circular viral M13 DNA plasmid reacting with about 200 synthetic oligonucleotides and self-assembling into the cross shaped DNA origami. Figure adapted from Seeman.²

In the original design of CO-01 by Seeman et al.,² the four arms of the CO are modified using two sets of 5 base pair overhangs, known as sticky ends. These sticky ends are designed to be complementary to each other and modifications can result in the generation of 1-D linear and 2-D planar arrays. DNA nanotechnology has largely made a remarkable impression with

nanostructures and nano-sensors on small, finite structures that can be configured to any shape or image.⁴ However, the other domain of how larger structures and objects are synthesized is still being investigated and is bridging the nanoscale features of DNA origami with the near microscale resolving power of optical microscopy.^{5, 6} These small nanostructures have size constraints that are limited by the applicable space within biological system such as nanorobots controlling cellular functions.⁷ The development of an economical synthesis method for longer sequences of DNA would significantly benefit efforts to synthesize structures on such a microscopic level. Although the micrometer scaled structures described in this thesis have not been produced commercially, the potential for inexpensive and reliable production of large complex systems using the micrometer building blocks we are developing exists. The synthesized 1-D and 2-D arrays of alternating cross origami can be modified to support the development of DNA detection devices.⁸ Since the 1-D and 2-D arrays are alternating between two different cross origami, optical reporters can be integrated on the cross origami allowing them to have a 200 nm separation which is just at the Abbe optical limit for microscopy. The design of the other 2-D array described here does not utilize the alternating cross origami; however, the 2-D array can be used in practice for micro mechanical belts.⁶ This would allow the electronic engineering community to have a building block to prototype larger components with commercially viable applications with transport mechanisms.⁶

This work focuses on the assembly of finite 1-D linear arrays and 2-D planar arrays through simple staple modifications. Using the complementarity of sticky ends similar to that described above, 1-D linear arrays and 2-D planar arrays can be designed to be constructed by alternating two different origami constructs (CO-01 and CO-3970) which are differentiated from each other through biotin-streptavidin and molecular beacon version 2 (MBv2) staple

modifications. To make the 1-D linear arrays and 2-D planar arrays finite instead of infinite, a second, specialized CO-01 and CO-3970 monomer is designed with 6 sequences of (polyT)₅ on the designated arm, which will terminate the polymerization of 1-D linear arrays and 2-D planar arrays to a predetermined length. In other approaches described in this work, attempts were made toward generating alternating 1-D linear arrays consisting of 8 monomers through titration methods and alternating 2-D planar arrays consisting of 8 monomers through gel electrophoresis methods. These alternating arrays were to be utilized as a platform to be modified with complexes known as molecular beacons, in our case called MBv2, for enhanced fluorescent imaging and detection of DNA/RNA target sequences.⁹

DNA Origami

DNA origami was invented by Paul Rothemund in 2006.¹ Rothemund DNA origami¹ is designed using two steps. The first step consists of engineering a geometric model of a target structure. Examples of the wide variety of possible shapes were shown in the Rothemund paper such as stars, smiley faces, and map of the world.¹ With the geometric model of the structure, the desired shape can be filled with an even amount of parallel double helices. Using periodic crossovers, the helices can be joined or cross-linked. Different types of junctions such as B-form DNA and Holliday junctions¹⁰ have helices that can be joined. B-form DNA is DNA that has a canonical right-handed DNA helix and is the most common form of DNA.¹¹ Holliday junctions are four-stranded antiparallel stacked-X form DNA.¹⁰ DNA origami usually employs the commonly found B-form DNA and has double helices that can be truncated to cut to complete a shape. The second step is to assemble the modeled construct by rastering a single long scaffold strand. The rastering technique is utilized such that the scaffold comprises one of the two strands in every helix. When the scaffold is rastered to join another set of helices, a “scaffold crossover”

is created. The scaffold used throughout this research is M13mp18. M13mp18 phage is propagated in *E. Coli* ER2738, purified by polyethylene glycol precipitation, and extracted with phenol.¹² It is a single-stranded, circular 7249 nucleotide sequence.

With Figure 1 information, Seeman² was able to create a cross-shaped DNA origami (CO). Many of the experiments described in this thesis utilized two types of CO. The first was created by Nadrian Seeman, CO-01, and the second was designed by Dr. Michael Norton, CO-3970. Like Rothemund's¹ origami, the CO is synthesized through an annealing process, in which about 200 short staple strands of DNA direct the folding of a long scaffold strand of DNA (M13mp18) into a flat array of antiparallel helices. In a rastering fashion, the DNA is folded into orthogonal rectangles. The two rectangles self-assemble orthogonally to create a cross shaped DNA. The difference between the two CO is that the Norton design was sequence optimized by Paragon Nanolabs, finding that the 3970th permutation of the base pair sequence was the best.

Biotin Binding to Streptavidin

Streptavidin is a tetrameric protein isolated from the actinobacterium.^{13, 14} Since biotin and streptavidin have the highest affinity for noncovalent interactions, the formation of a nearly irreversible and specific linkages are enabled between these biological macromolecules. Using two biotin modified staples, the Norton lab was able to consistently label CO with streptavidin. Since CO-01 and CO-3970 are identical when imaged on the AFM, a staple strand in the CO is modified to have a biotin molecule at the 3' or 5' end. Streptavidin is then added to the solution allowing the binding of streptavidin to biotin to allow visualization of a topographic difference between the two COs when imaged with an AFM.¹⁵

Superresolution Microscopy

By overlaying the Fast Scan Atomic Force Microscope (AFM) image and the fluorescence microscope image, a model distribution of light can be obtained and used for calculations in super resolution imaging, surpassing Abbe's Limit. In Figure 2, the FastScan AFM is located on top of the fluorescence microscope to allow for the overlaying of the AFM image and fluorescence image.

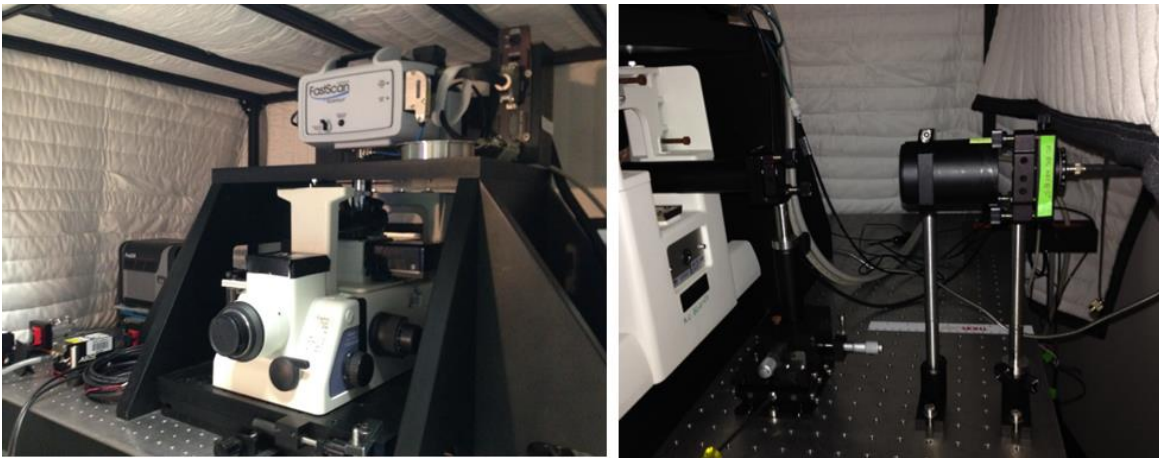


Figure 2. Fast Scan AFM and Fluorescence Microscope. Depiction of the fast scan AFM and fluorescence microscope that the Norton lab utilized for imaging of sensors on DNA origami arrays.

Abbe's theory states "interference between 0th and higher order diffracted rays in the image plane generates image contrast and determines the limit of spatial resolution that can be provided by an objective".¹⁶ In layman's terms, normal optical microscopy has a resolution limit of about 200 nanometers (nm) for the shortest wavelengths of visible light. This can be expressed in the below equation.¹⁷

Abbe's Law $d = \frac{\lambda}{2NA}$

*d = resolving power
λ = wavelength of light
NA = numerical aperture
N = refractive index of the medium between the objective and the cover glass
A = angle aperture*

Equation 1.

Thus, individual copies of our molecular beacon, MBv2, can be imaged under certain conditions. MBv2 was inspired by the design of Jockusch et al.¹⁸ Molecular beacons “are specifically designed DNA hairpin structures that are widely used as fluorescent probes”.¹⁹ In its uncomplemented form, MBv2 is a molecular beacon with a hairpin structure that has both Cy3 and ATTO647 as its two fluorophores. In its uncomplemented form, the fluorescence microscope will identify ATTO647 as the emitter of light. However, if the complement to the uncomplemented MBv2 is added, the hairpin structure is straightened, and Cy3 is released from energy transfer and emits. With these probes, fluorescence resonance energy transfer (FRET) is utilized as their signal-transduction mechanism. According to the Jablonski diagram in Figure 3, the effect of fluorescence can be displayed.

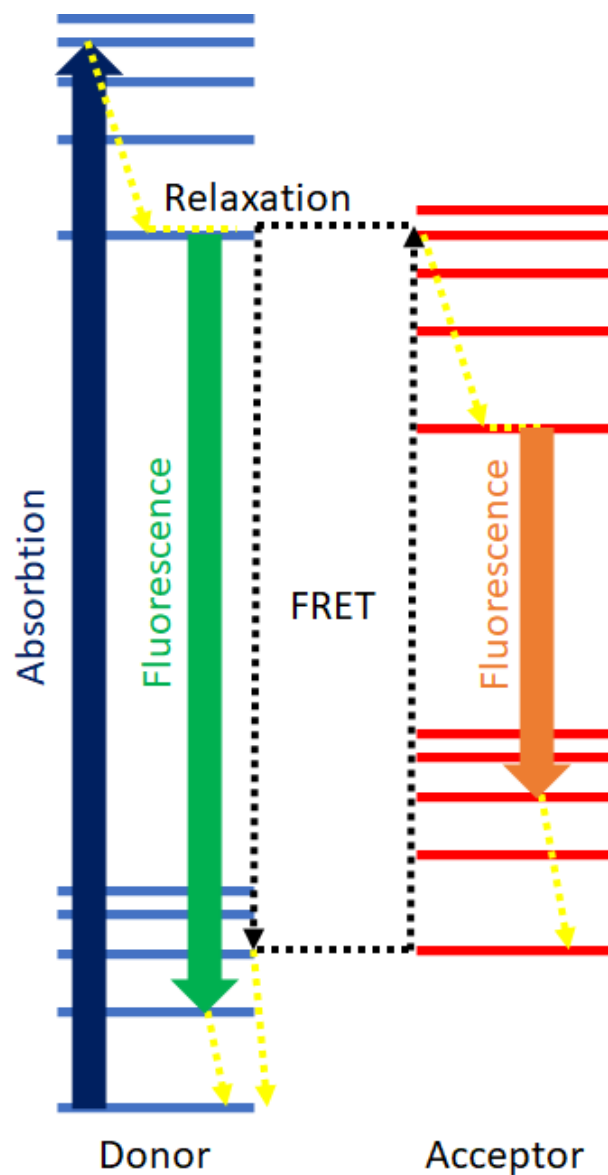


Figure 3. Förster Resonance Energy Transfer. Illustration²⁰ of the transfer of the electronic excitation energy within the donor fluorophore to the acceptor fluorophore and decay.

As the fluorophore interacts with a photon with a specific wavelength, the electron within the fluorophore is raised to an excited energy state. Once it reaches that excited state, the electron drops to lowest vibrational level of the excited singlet state through vibrational relaxation. This occurs within a few picoseconds. Emission from this excited singlet state can occur in a few nanoseconds since the excited electronic state is very unstable. In the case of a molecular beacon, since the distance between donor and acceptor is increased upon addition of

complement, there will be a decrease in FRET on target DNA capture. The target DNA can be identified by the change in fluorescence and proved that FRET can be used as an efficient signal-transduction mechanism.

Characterizing Plasmon Spectra for Assemblies

By utilizing the CytoViva enhanced darkfield microscope,²¹ plasmonic spectral shifts can be utilized to characterize assemblies of 40 nm gold nanoparticles (AuNP). AuNPs were chosen due to their stability and processability in high ionic strength buffers used for DNA manipulation and identification.²² Instead of attaching the AuNPs to terminal thiols on the oligonucleotide,²³ a DNA-dendron conjugate was synthesized. Using a procedure developed by Day et al.,²² a G2 PAMAM dendrimer (structure shown in Figure 4 below) was cleaved and attached to a functionalized and modified DNA strand complementary to our CO-01.

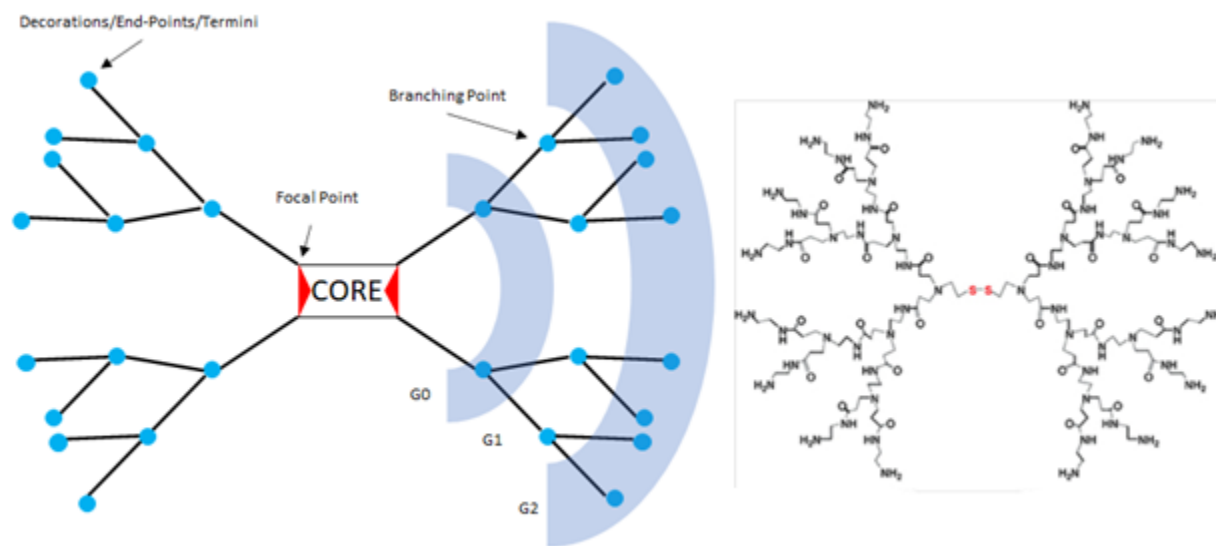


Figure 4. G2 PAMAM Dendrimer. G2 structure, which illustrates the 16 primary amines surrounding the cystamine core.²⁴

Since the larger objective is to characterize the plasmonic spectral shift accompanying dimerization of two 40 nm AuNP's, a second 40 nm AuNP was to be attached to a long tether via

dendrimer. Using a complementary sequence/strand, the tether can attach/immobilize the second 40nm AuNP beside the first stationary 40nm AuNP.

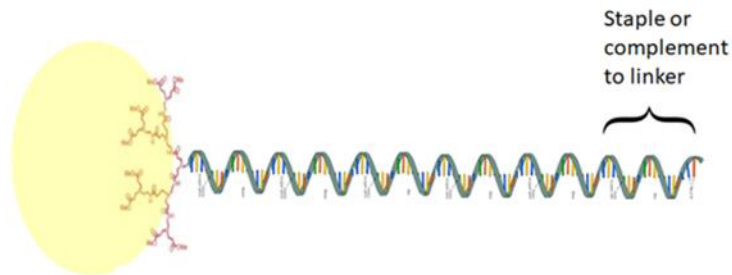


Figure 5. Modular parts of the Refined Dendron to Conjugated DNA with a Long Tether. Illustration of the linkage of the construct with the origami.

Thus, creating a plasmonic spectra shift. Modeling performed by Juluri et al.,²⁵ demonstrate that plasmonic spectra shift can be computed. However, this modelling must be corroborated with experimental evidence. The experimental setup we proposed would be to use the CytoViva darkfield microscope to characterize the scattering²¹ to observe the spectral shift from 2 separate 40 nm AuNPs and 2 side-by-side 40 nm AuNPs.

CHAPTER 2

PROPOSED APPROACH AND DESIGN

With a basic understanding of what DNA origami is, the design aspect of creating different substrates can be implemented. Since DNA origami can be modified with different types of sensors, these constructs could enable studies using super resolution techniques and characterizing plasmon spectra for assemblies to be conducted. However, since the sensors themselves provide sufficient data about their fluorescence and plasmon spectra in bulk/ensemble measurements, the implemented DNA arrays should be designed to enable the sensor structures to be viewed individually with optical microscopy.

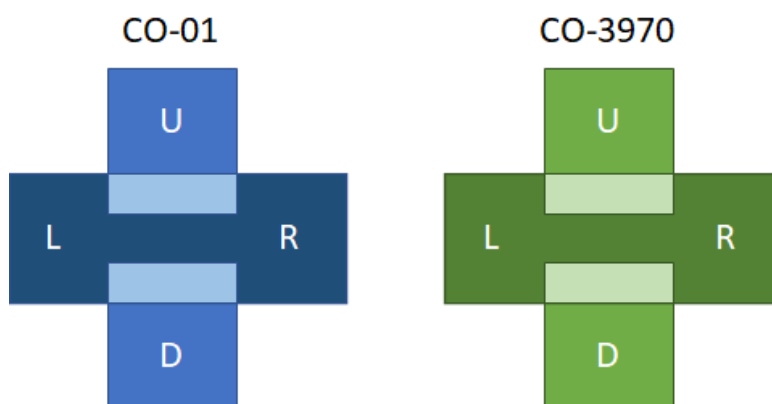


Figure 6. Legend of Illustrated CO. Representations used in this thesis: the blue CO on the left represents CO-01 and the green CO on the right stands for CO-3970.

Our goal was to produce 2 major DNA origami substrates that can be adapted to use either a molecular beacon or gold nanoparticle. Since staples within the DNA origami can be modified, the distance between sensors can provide the potential to observe individual “on” and “off” signals. Capable of detecting a single analyte molecule, several staple sequences were modified to enable molecular beacons and gold nanoparticles to be positioned at specific distances away from each other.

The first design consists of a 1-D alternating array with CO-01 having a modification on the left arm. With the idea of creating a 200 nm distance between each molecular beacon, this spacing would be consistent with Abbe's Law and allow us to employ traditional optical microscopy for the shortest wavelengths of visible light (Figure 7). This use of non-super resolving techniques would reduce the complexity of systems necessary to see each fluorescent reporter individually.

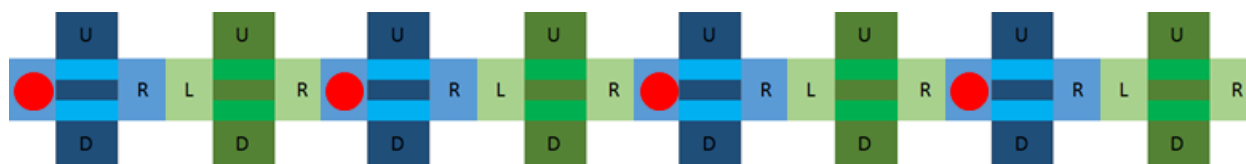


Figure 7. Design of Alternating 1-D Linear Array of CO-01 and CO-3970 with MBv2 on the Left Arm of each CO-01. This positions the MBv2's at 200 nm separation. UDLR indicates the up, down, left, and right arm. Red circles are MBv2.

The second design consists of a dimer of origami, which would be a sub-component of a 2-D array with 40 nm gold nanoparticles on the up arm of the CO-01 and on a tether on the down arm of CO-3970 creating an “on” and “off” system with the 40 nm gold nanoparticles displaying a plasmon spectral shift during the binding of analyte. With the addition of a target sequence, the tethered 40 nm gold nanoparticle on CO-3970 would be bound beside the stationary 40 nm gold nanoparticle on CO-01 thus causing a spectral shift. The objective of this part of the project was to produce a DNA-Dendrimer construct capable of binding a 40 nm gold nanoparticle, as shown diagrammatically in Figure 8.

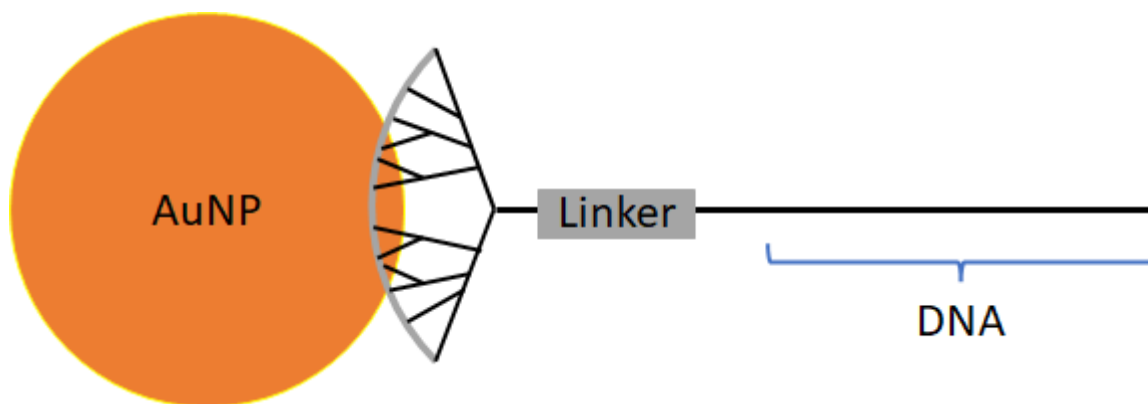


Figure 8. Dendron to Conjugated DNA. Illustration of the modular design attaching a 40 nm AuNP to a dendron to a linker to a DNA strand that could be added to CO-01.

CHAPTER 3

0-D AND 1-D ARRAYS

The basic folding paths and structures of the two main CO Designs used in this thesis are shown and described below.

CO-01

The original cross origami was designed by W. Liu et al.² and is called CO-01

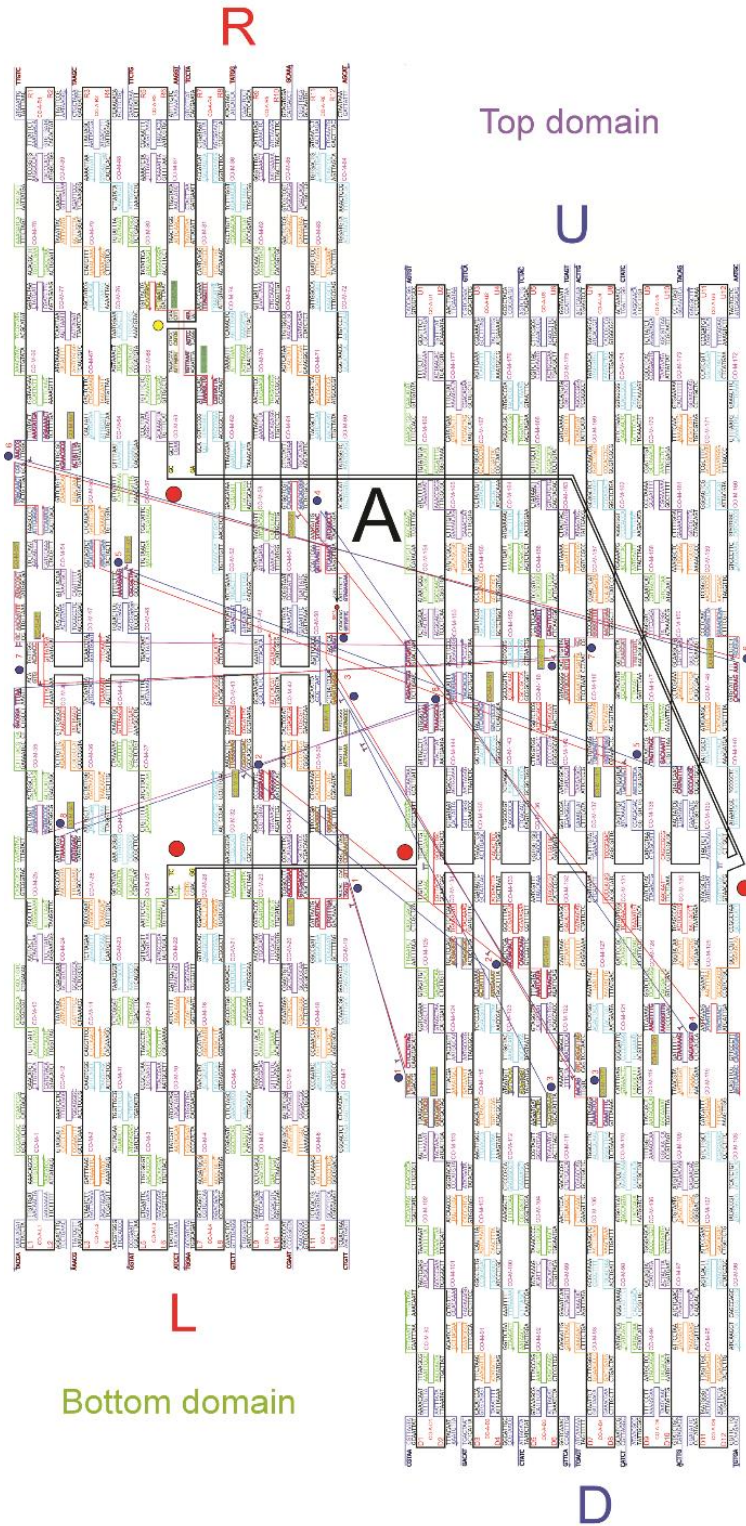


Figure 9. CO Map of CO-01. Illustration of the M13 scaffold and 201 short staple sequences self-assembling into two orthogonal rectangles to create the CO-01. Figure adapted from Seeman.²

CO-3970

The original cross was modified from the W. Liu et al.² designs by Dr. Michael Norton, producing candidate permutations by incrementing the location of the zeroth base through the structure. The optimal base pair sequence was the 3970th permutation.

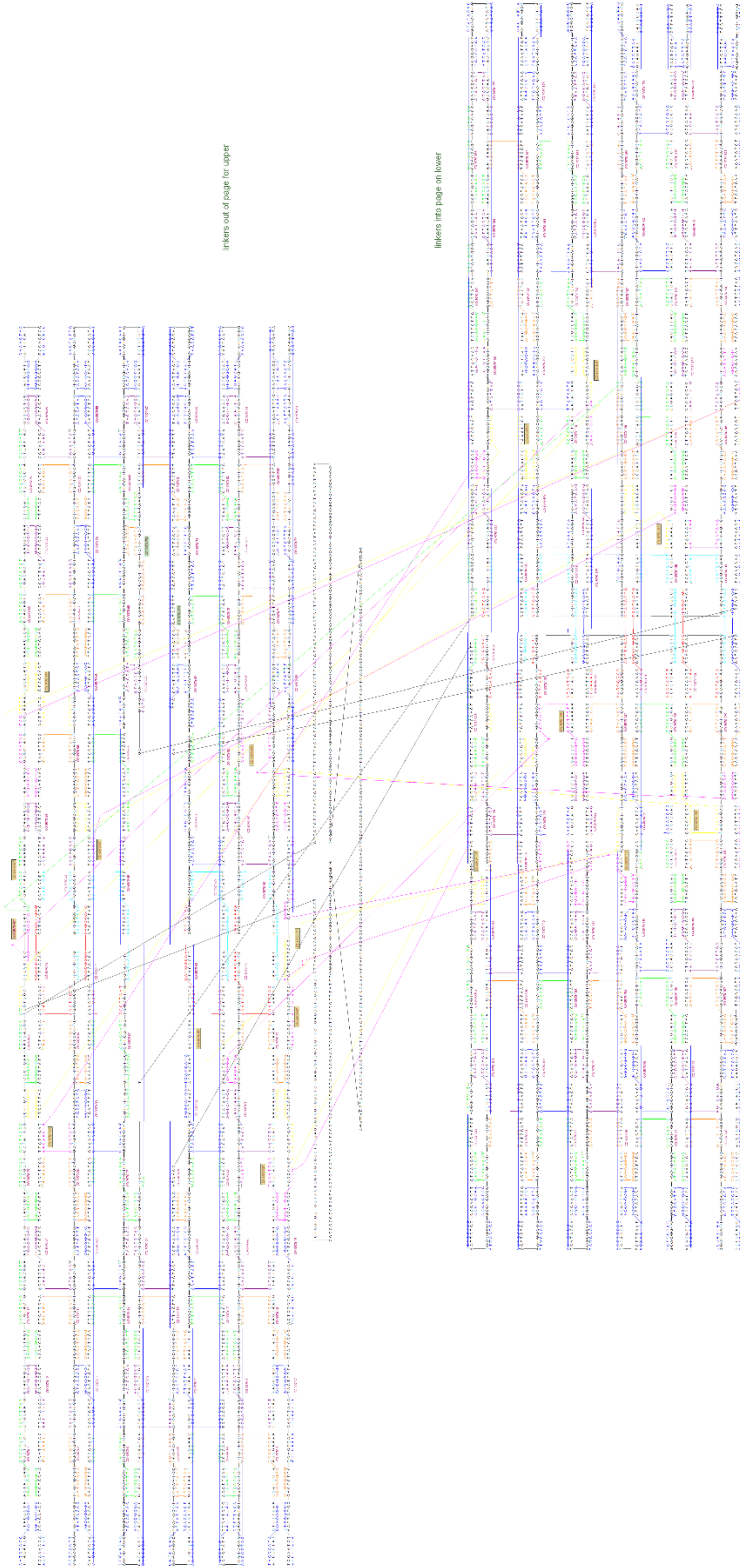


Figure 10. CO Map of CO-3970. Illustration of the M13 scaffold and 201 short staple sequences self-assembling into two orthogonal rectangles to create the CO-3970 structure.

Types of Origami Junctions

After the invention of origami, W. Liu et al.² and Rothmund et al.¹ demonstrated the interaction between helical stacking in origami-to-origami interactions. Since origami do not readily stack on top of each other and do not align themselves perpendicular to the direction of the helices, interactions between edges of origami can be utilized to synthesize multiple origami constructs aligned parallel to the helical direction.

In the original design of W. Liu et al.², the arms of a cross origami were extended from the core using two sets of 5 base pair overhangs. Their arrays utilized two identical cross origami core structures bound together by “sticky ends”. However, the Norton lab utilized base pair overhangs complimentary to the M13 scaffold of the second type of origami instead of binding to another base pair overhang.

Before the current research, the sticky ends used in the Norton lab were 3 nucleotide-long interdigitations. Due to many difficulties with synthesizing “infinite” 1-D alternating arrays, the sticky ends were redesigned to a 5 nucleotide-long overhang, as illustrated in Figure 11. This allowed the growth of nonfinite 1-D alternating arrays to form beyond the 3 to 4 monomer long arrays previously imaged. With 17 being the longest array imaged, we considered the change to be a success.

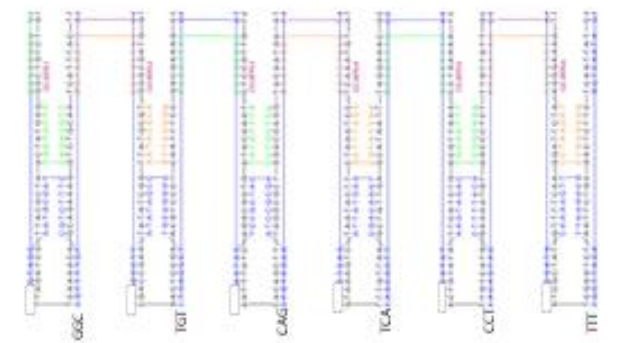
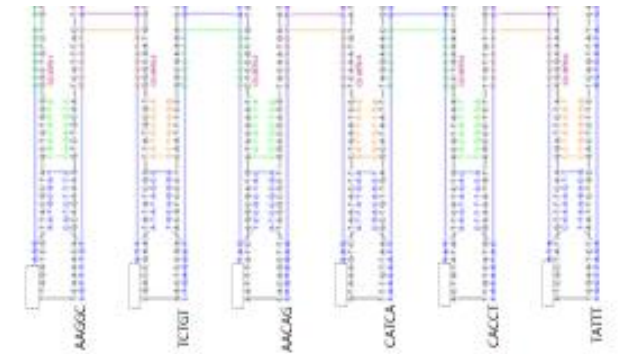
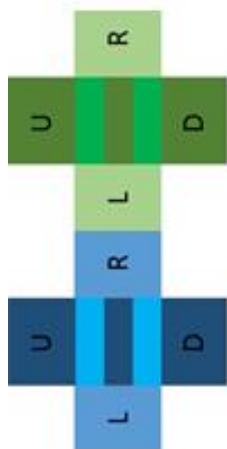
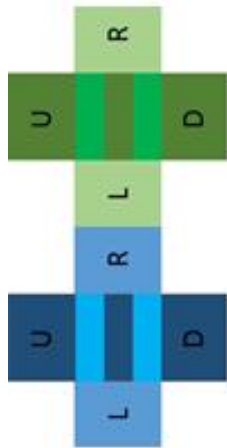


Figure 11. 3 BP SE Overhang vs 5 BP SE Overhang. Illustration of the change in the transition from 3 BP SE overhangs to 5 BP SE overhangs to ensure better array growth.

Infinite vs Finite 1-D Arrays

When creating 1-D structures, CO is assembled by utilizing sticky ends to attach one arm of one CO to another arm of a different CO. The assembly of infinite 1-D arrays is a simple task. Prior to this experimentation in the Norton lab, infinite arrays were synthesized by mixing all the staples together at the same time and annealed once. In this work, CO is pre-synthesized and mixed with sticky ends specific to the attachment of one arm to another arm of a different CO. When imaged on an AFM, the results should yield multiple lengths of 1-D arrays. Typically, the lengths of the “infinite” 1-D arrays are 10-mer and longer with occasional shorter arrays present. This can be seen in Figure 12.

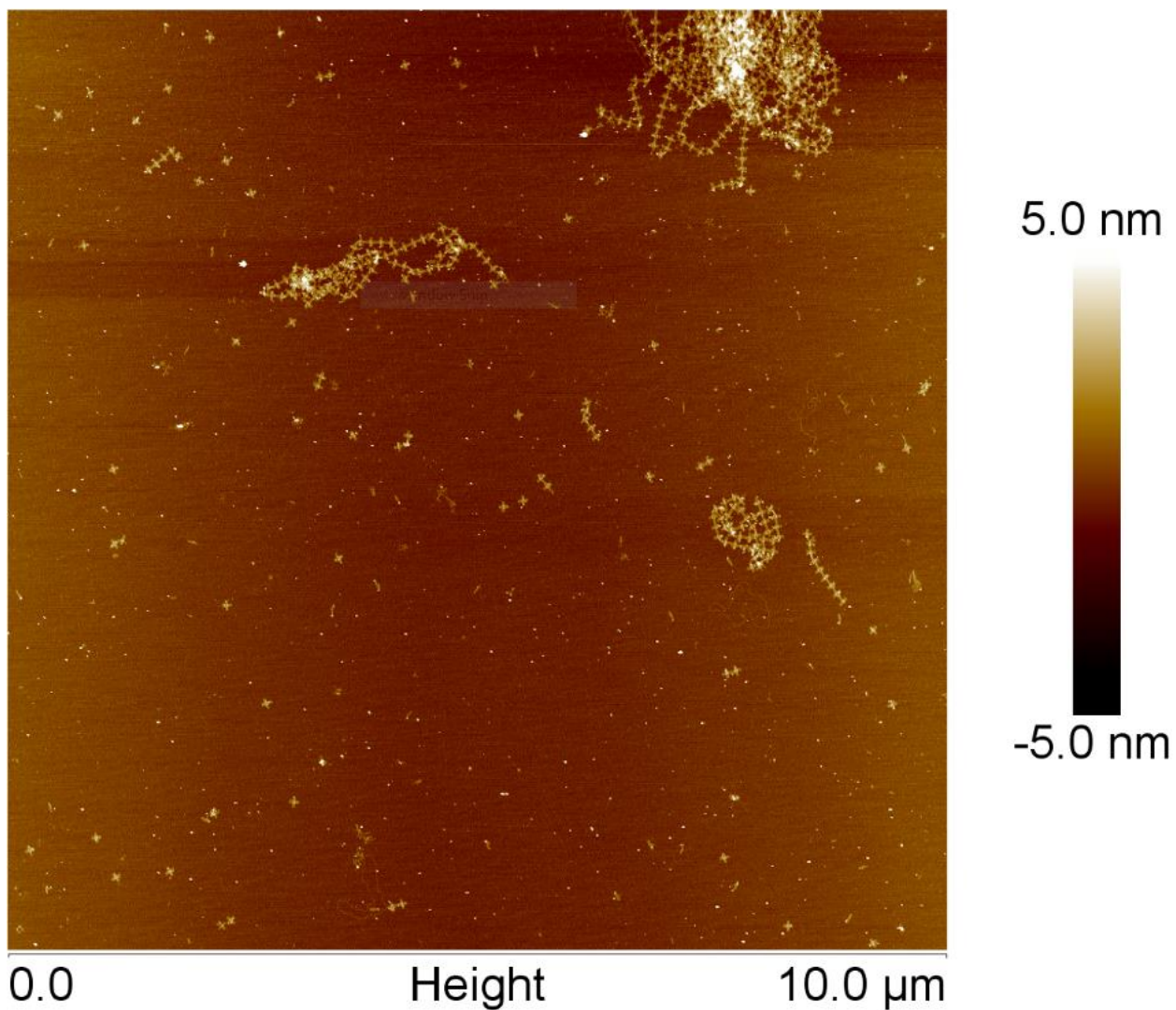


Figure 12. AFM Image of “Infinite” 1-D Arrays.

Figure 12 shows “infinite” 1-D arrays with varied lengths. Although infinite 1-D arrays can be consistently synthesized with favorable yields, having 1-D arrays with “infinite” length for this research was not desired due to potential for aggregation. Instead, the synthesis of finite 1-D arrays was desired.

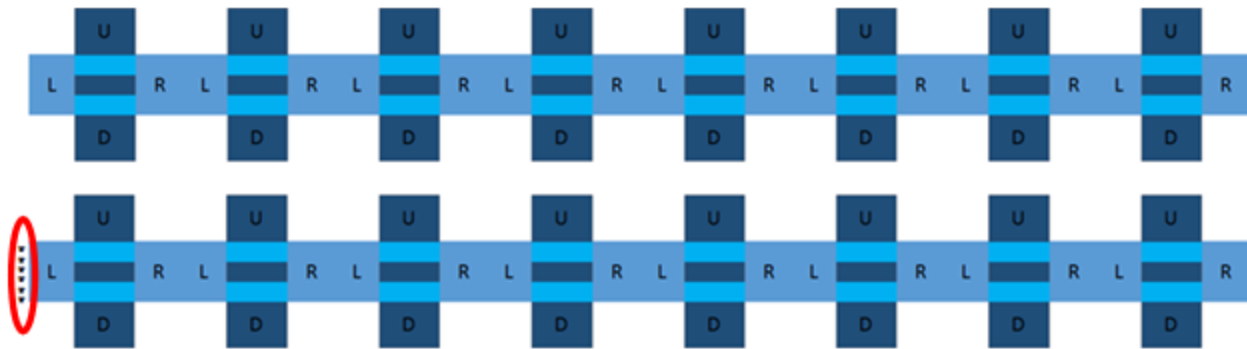


Figure 13. Infinite vs Finite 1-D Arrays. Illustration of the design of a 1-D array and the difference between infinite and finite 1-D arrays with six 5 poly T's on left arm of the far left CO.

The major difference between infinite and finite 1-D arrays is the presence of terminated sticky ends on one arm as a proportion (e.g. 1:10) of the CO in a finite 1-D array. Since one arm is “terminated” with six 5 T ends, the growth of the 1-D arrays in a one-pot (preformed CO with SE) synthesis can be stunted to create shorter arrays instead of the 10-mer and longer 1-D “infinite” arrays. This is represented schematically in Figure 13.

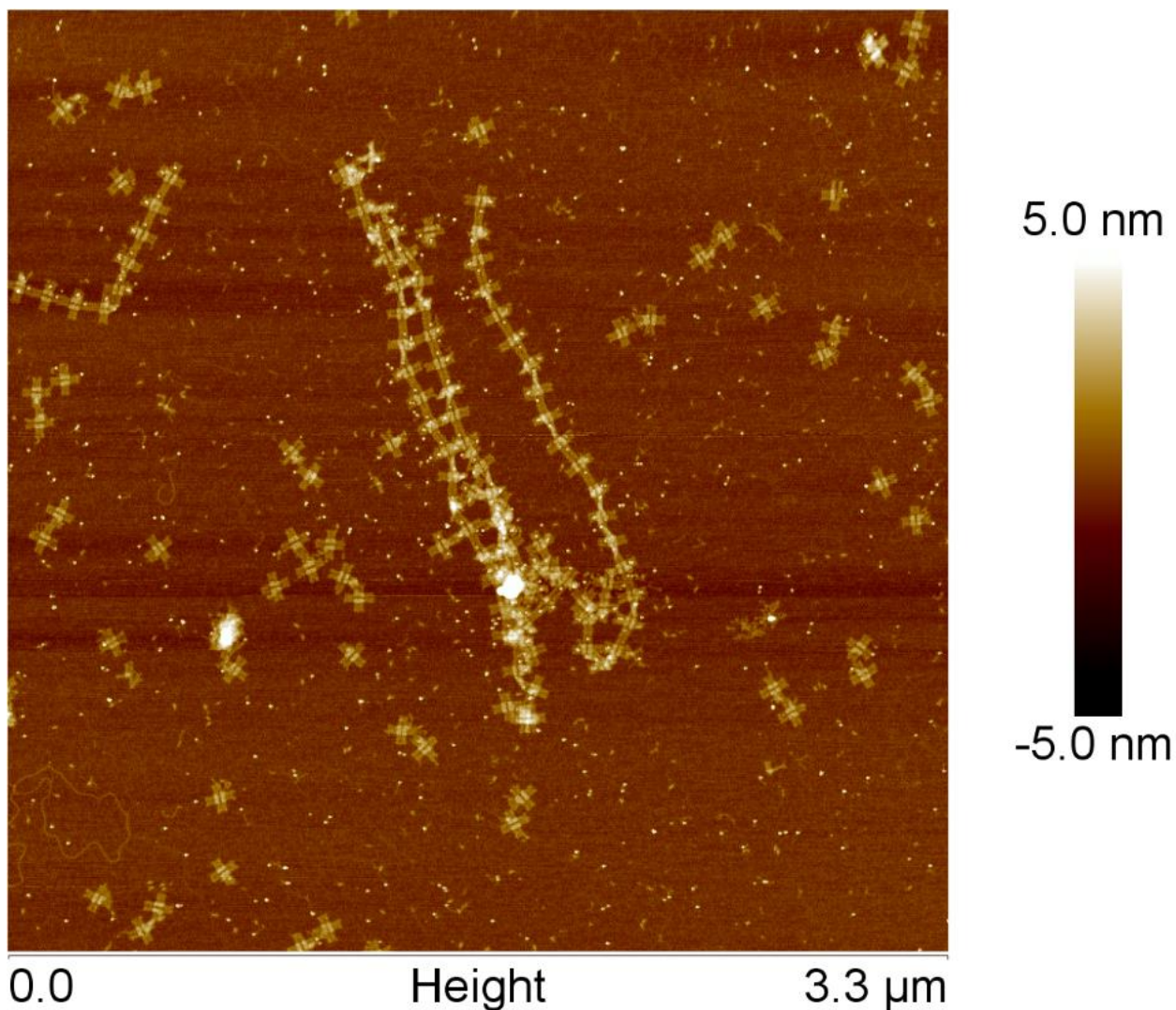


Figure 14. Finite 1-D Array. AFM image of finite 1-D arrays where the CO-01 T is labelled with Streptavidin on the left and right arm while CO-01 is labelled with Streptavidin on the left and down arm.

As shown in the AFM image (Figure 14), the length of the finite 1-D arrays are generally much shorter than 10-mers. The length of the finite arrays can be manipulated using the ratio of terminated CO to non-terminated CO. However, this is not a deterministic technique but can produce acceptable results based on probability.

Parallel vs Rotated 1-D Arrays

Another design characteristic of 1-D arrays is the production of parallel vs rotated 1-D arrays. When observing any image of CO, for example in Figure 14 above, one can see an “equal sign” like shape in the middle of the CO. The “equal signs” form due to two double helices stacked on top of each other when the rectangular subunits are stacked together.

Depending on the orientation of the “equal sign” in the middle of the CO in a 1-D array, the 1-D array is either parallel or rotated.

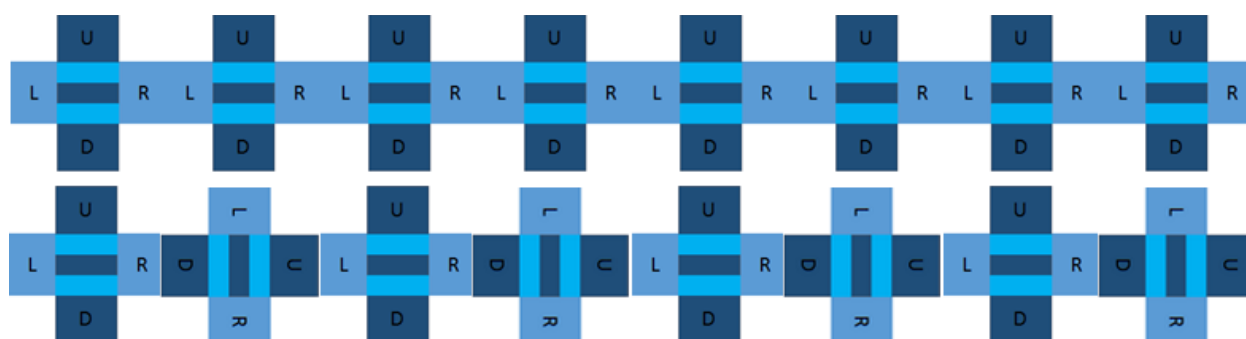


Figure 15. Parallel vs Rotated 1-D Arrays. In this illustration the “equal sign” in the middle of the CO is all parallel in the top 1-D array but the “equal sign” is rotated by 90° in the bottom 1-D array.

Alternating vs Homogeneous 1-D Arrays

The final characteristic of 1-D arrays is homogeneous vs alternating 1-D arrays. The simple description to enable one to differentiate between the two 1-D arrays is that homogeneous 1-D arrays use only one type of CO while alternating 1-D arrays use two different types of CO. Similar to the manner in which homogeneous 1-D arrays are created with sticky ends, alternating 1-D arrays also use sticky ends to connect the left and right arms of the two different subtypes of CO.

When creating a homogeneous 1-D array, CO is assembled by utilizing sticky ends to attach one arm of one CO to another arm of the same subtype of CO. When imaged on an AFM, the results should yield a one-dimensional structure composed of only one type of CO.

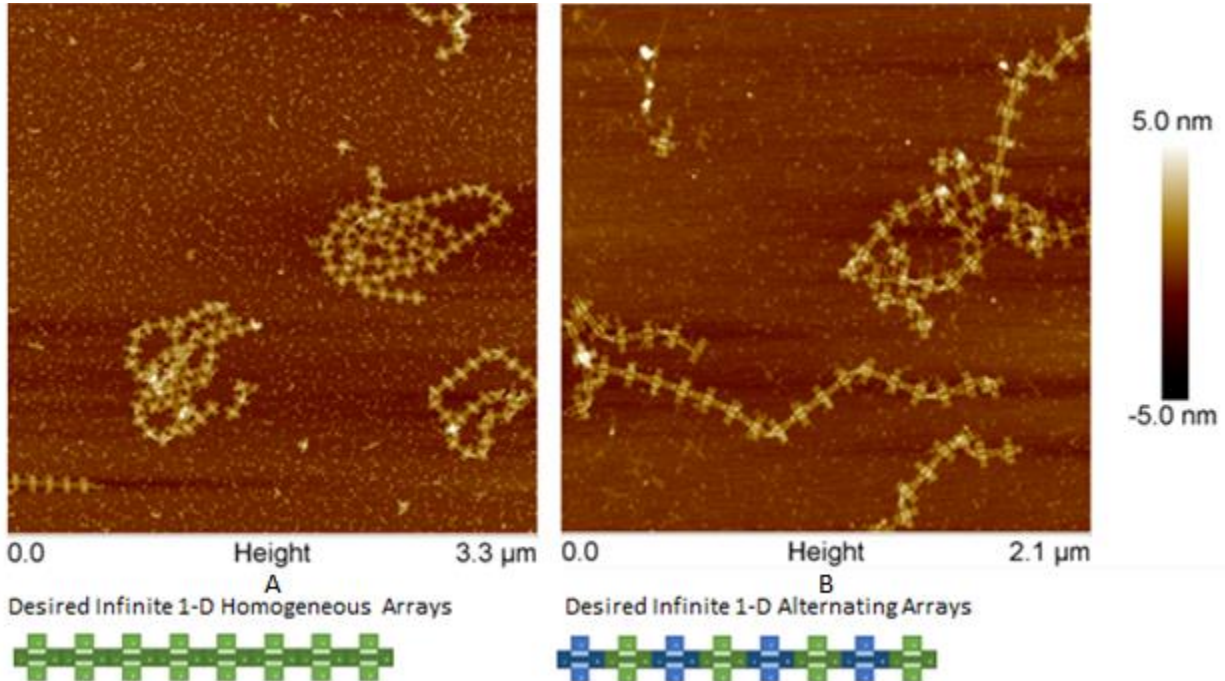


Figure 16. Homogeneous vs Alternating 1-D Arrays. AFM images and associated representations of the difference between homogeneous and alternating arrays. Figure 16 A depicts homogeneous 1-D arrays. Figure 16 B depicts alternating 1-D arrays.

Figure 16 A shows a homogeneous 1-D array with only one type of CO. Since the synthesis of homogeneous 1-D arrays has been performed with some success, as indicated by the length of the products in Figure 16, the synthesis of alternating arrays was attempted next.

CHAPTER 4

2-D ARRAYS

Infinite vs Finite 2-D Arrays

Like infinite vs finite 1-D arrays, infinite vs finite 2-D arrays are also distinguishable by the terminated left arm of the far-left CO. However, instead of a single linear array structure, this structure is the simplest multidimensional array, consisting of two parallel linear arrays combined into one structure. Throughout this research, the up arms of CO-01 and down arms of CO-3970 are mostly terminated to prevent growth vertically.

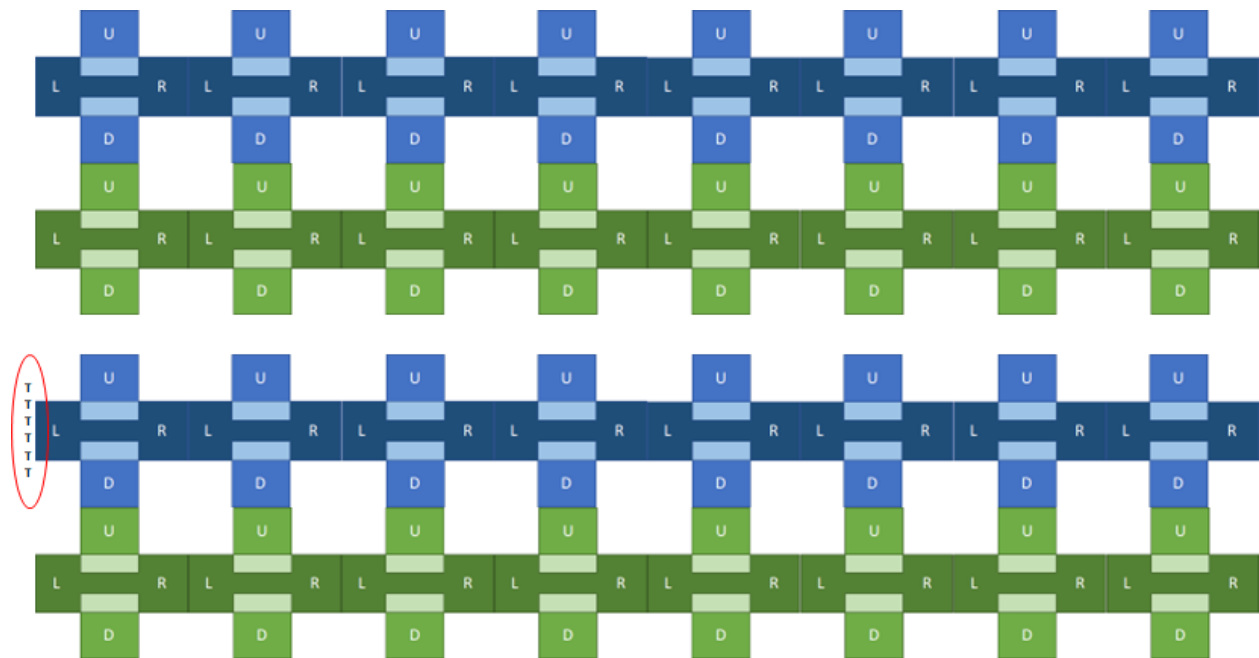


Figure 17. Infinite vs Finite 2-D Arrays. Illustration of the coupled linear structures comprising of 2-D arrays. The upper 2-D array is infinite whereas the lower 2-D arrays are finite due to the terminated left arms of the far-left COs.

Parallel vs Rotational 2-D Arrays

For microscopic confirmation of parallel vs rotational 2-D arrays, the “equal signs” in the CO are inspected. Figure 18 illustrates the orientation of the “equal signs” that determine whether the 2-D array is parallel or rotational.

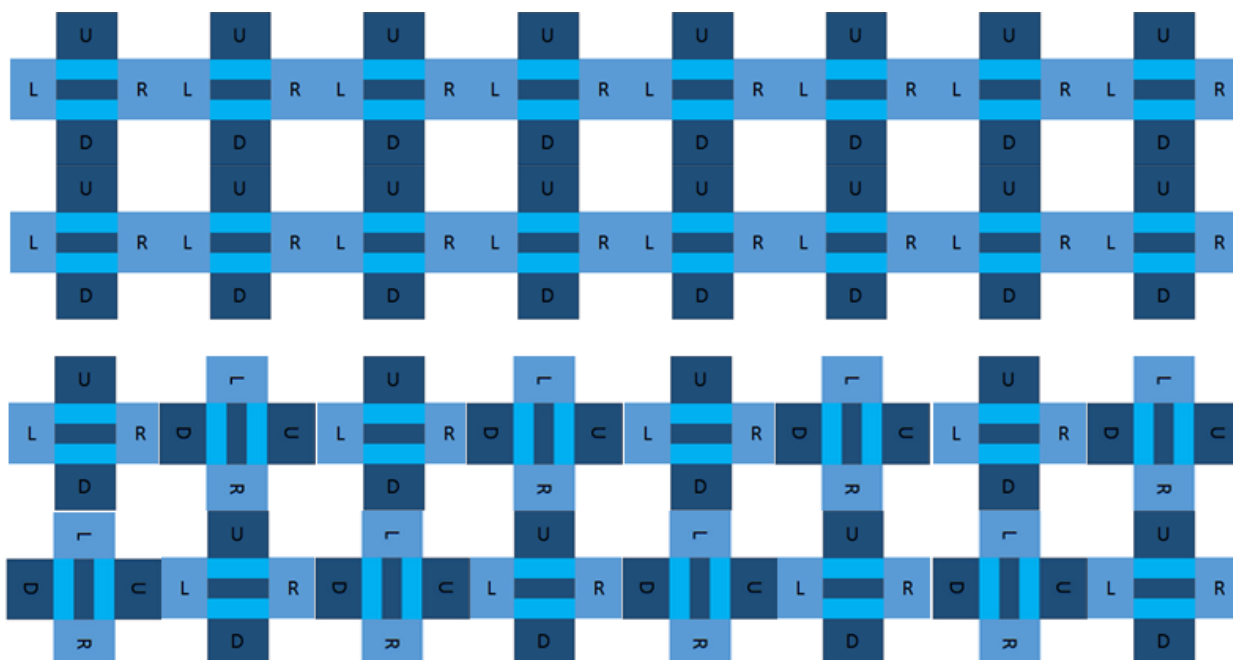


Figure 18. Parallel vs Rotational 2-D Arrays. Illustration of the rotational 2-D array in which some of the COs are rotated 90°.

When inspecting the lower 2-D array, one can see the 2nd, 4th, 6th, and 8th CO is rotated 90° in the upper portion of the 2-D array. The 1st, 3rd, 5th, and 7th CO are rotated 90° in the lower portion of the 2-D array. Only the parallel type of array was developed in this work.

Homogeneous vs Alternating 2-D Arrays

The difference between homogenous and alternating 2-D arrays is similar to homogenous and alternating 1-D arrays. The difference is that the homogenous 2-D array has only one type of CO and the alternating 2-D array has two subtypes of CO. In Figure 19, the top 2-D array is homogeneous or consists of only CO-01. However, the bottom 2-D array is heterogeneous due to having two different COs, CO-01 and CO-3970.

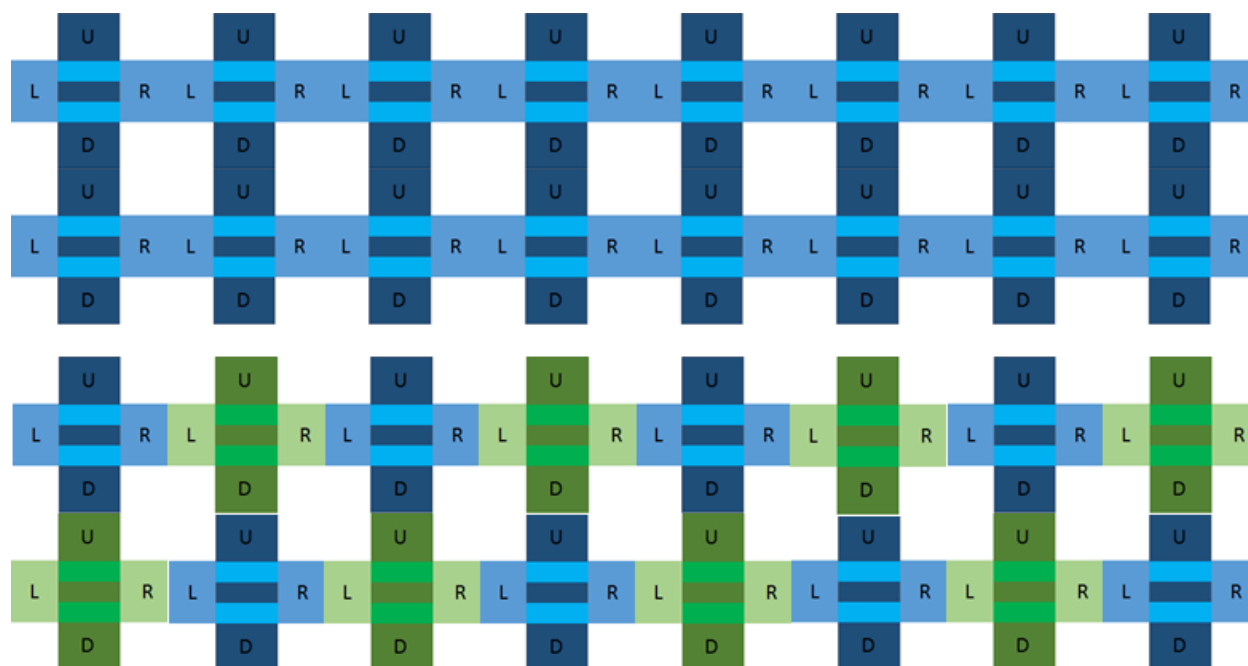


Figure 19. Homogeneous vs Alternating 2-D Arrays. Graphical representation of the alternating 2-D array in which there are two different types of COs that are self-assembled in an alternating fashion.

CHAPTER 5

MODIFICATION SITES

Biotin and Streptavidin

Biotin and streptavidin are commonly used in biochemistry for protein and nucleic acid detection and purification methods; however, this work uses the biotin-streptavidin interaction as a topographic indicator to show the difference between CO-01 and CO-3970. When imaging using the AFM, CO-01 and CO-3970 are indistinguishable. Thus, biotin modified staples are substituted in the short staple strands to direct a streptavidin interaction allowing us to see a topographic difference. Examples of this topographical differentiation are shown in Figure 20.

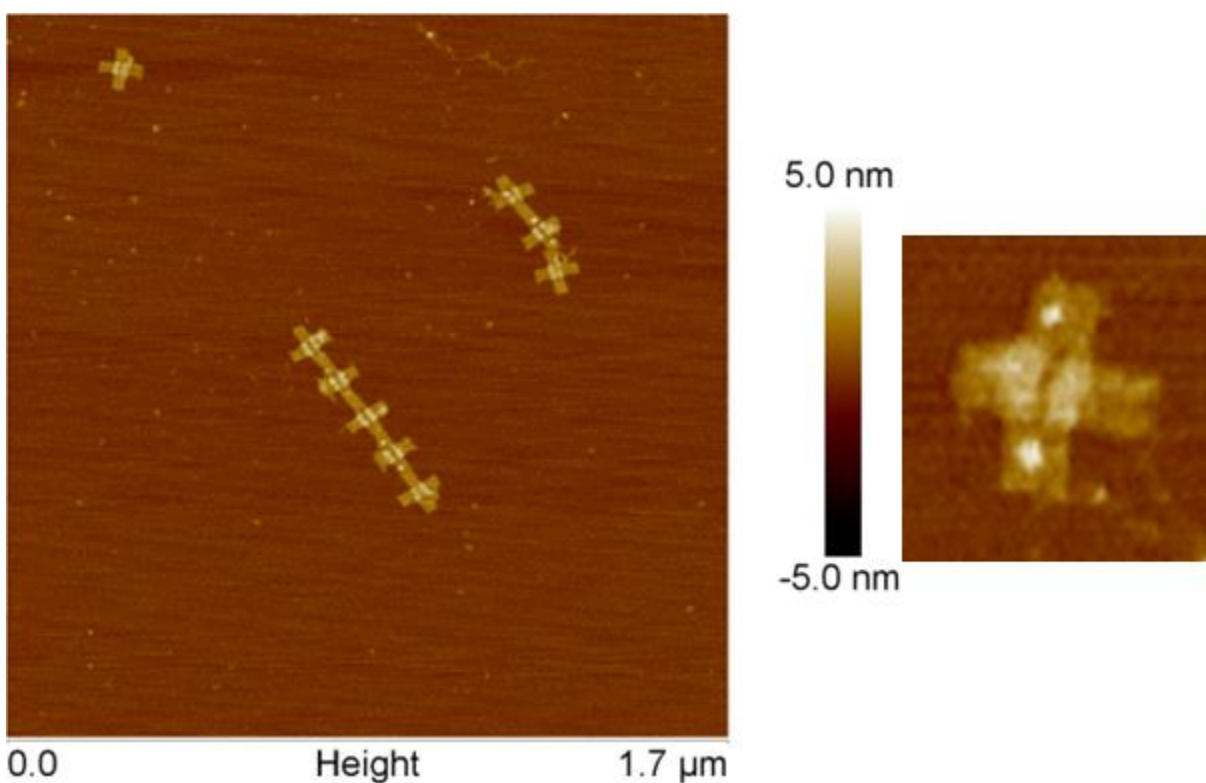


Figure 20. CO-01 with Streptavidin Labeling on the Left and Right Arms. AFM images of CO-01 with biotin modified staples on the left and right arms after decoration with Streptavidin in an alternating array. In the AFM image, one can clearly differentiate which COs are CO-01 and which are CO-3970 since CO-01 captures Streptavidin on the 2 biotin modified staples on the left and right arms.

Figure 21 shows possible locations where biotin modified staples can be added to CO-01. Not all locations are used in all sub-unit COs. Although maps appear flat (without depth), we understand that the 3D structure of DNA must be considered in selecting locations for biotin recognition by Streptavidin.

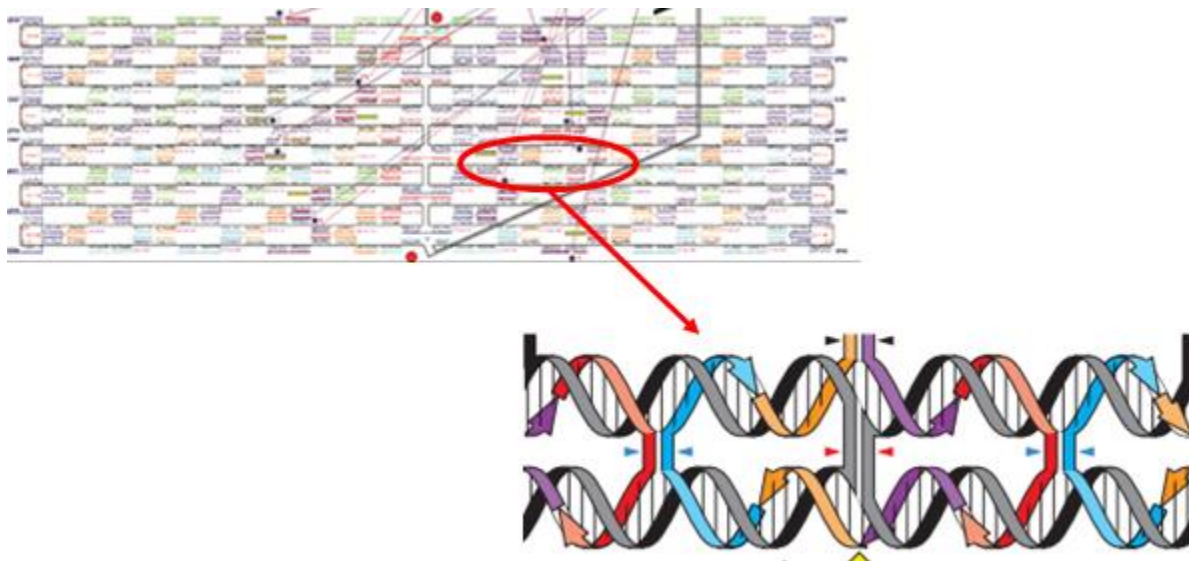


Figure 21. Helical Structure of DNA. Illustration of the helical structure of DNA and how the 5' and 3' ends can point out, in, or to the sides of the page. Main XY plane of the CO which is normally parallel to page in design maps. Figure adapted from Rothmund ¹ and Seeman.²

Figure 21 illustrates how DNA is a helical structure and that the 5' and 3' ends can point out, in, or to the sides of the page. Thus, when designing modifications for the CO, the orientation of the 5' and 3' ends of DNA is important to ensure that the modification is pointing out for maximum binding and therefore labeling probability. Figure 22 indicates commonly used staples where a biotin modified staple is added for streptavidin decoration.

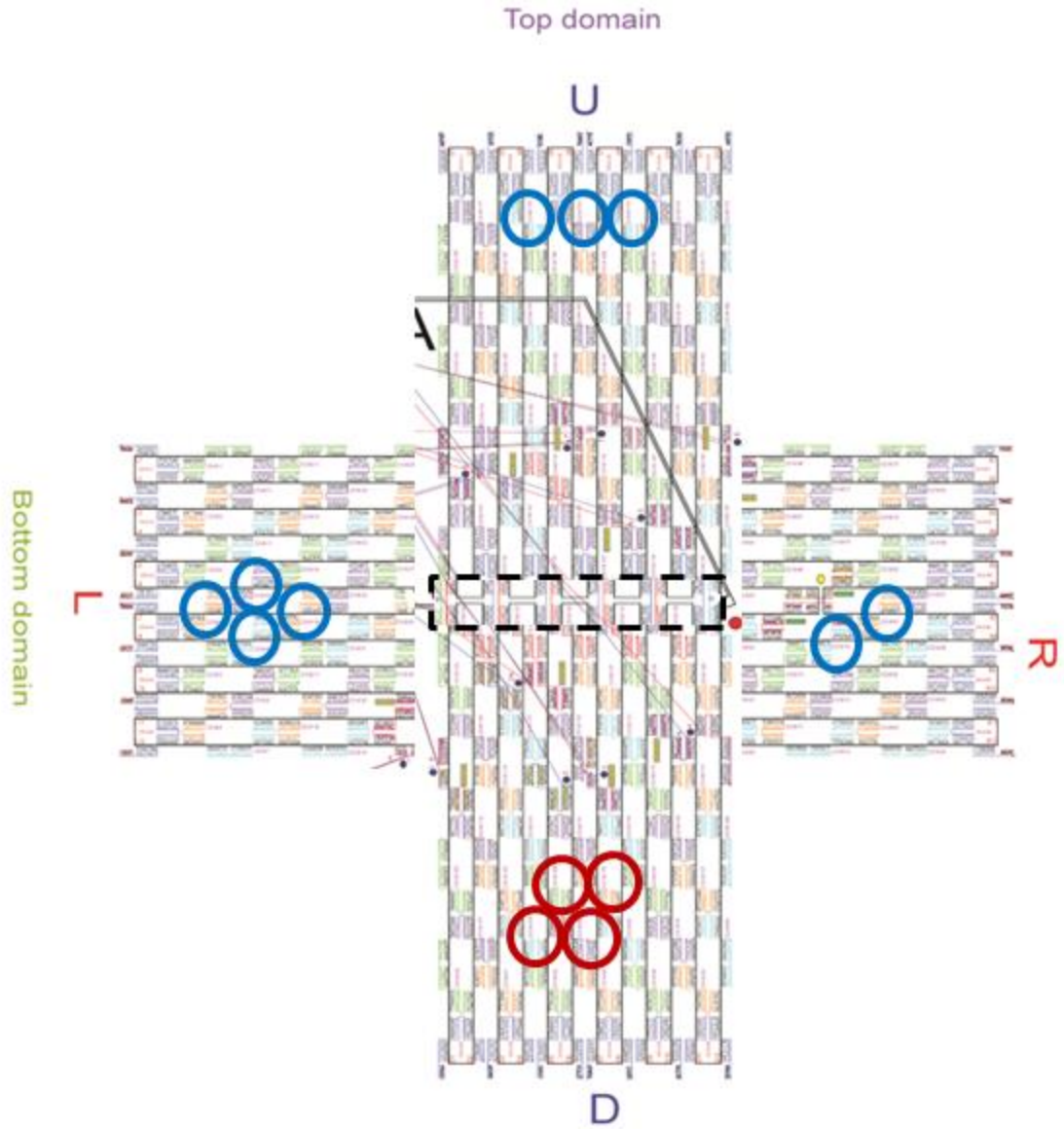


Figure 22. Biotin Modified Staple Sites on CO-01. Diagram depicting the different staple ends that have been analyzed to be “facing up” for use as biotin modified staples.

Molecular Beacon (MBv2)

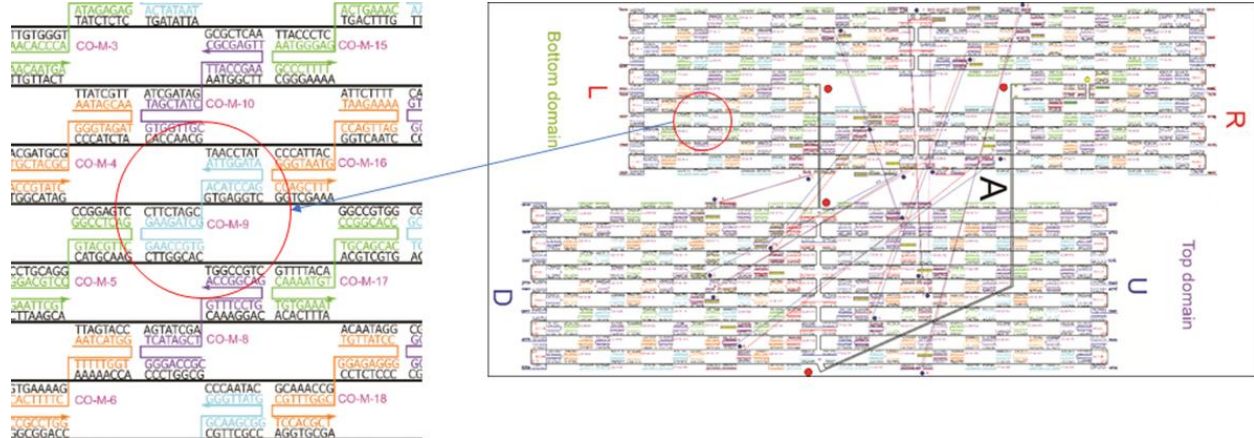


Figure 23. Design of MBv2 Implemented into CO-01. Staple CO-M-9 (circled) was modified with MBv2 at the 3' end so that the molecular beacon is “facing up” out of the page.

MBv2 is a unique molecular beacon that was designed by Dr. Michael Norton and has two fluorophores on one DNA strand. The uncomplemented form has a “hairpin” structure that only allows emission of ATTO647 fluorophore. However, when the complement to the MBv2 strand is added, the hairpin structure becomes open and the fluorophore Cy3 emits light instead.

Gold Nanoparticle (AuNP) with Dendrimer

The gold nanoparticle was initially designed to be on the up arm of CO-01. Figure 24 below shows the design in which staple 175 of CO-01 was selected and would be modified to have a dendron attached.

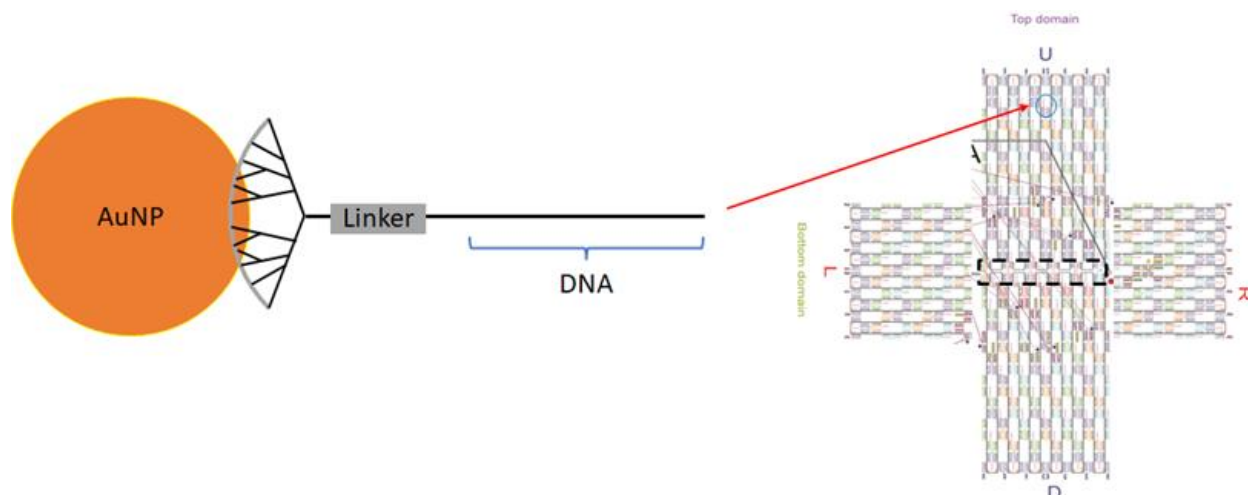


Figure 24. Design of Gold Nanoparticle and Dendron into CO-01. Illustration of the location of staple 175 was synthesized with a dendron at the end so the gold nanoparticle is “facing up” out of the page and therefore out of the plane of the CO.

Unlike MBv2, the dendron is synthesized to the conjugated DNA strand and then replaces the original staple 175. When changing the original staple sequence to the modified staple, the original staple is simply left out of the synthesis solution. This dendrimer-modified strand would be included in the annealing procedure. An alternative method for installing the modification would involve DNA strand-displacement. DNA strand-displacement can be used when two strands with partial or full complementarity hybridize to each other.²⁶ Although this mechanism would enable the dendron/AuNP complex to be added after CO is annealed, this mechanism was not employed due to anticipated complexity and expected slow kinetics

CHAPTER 6

METHODS

CO Monomer Synthesis

For the construction of the CO monomers, two sources were used for the DNA components. Bayou Biolabs (4724 Hessmer Avenue Metairie, LA 70002) provided the single-stranded M13mp18 DNA plasmid scaffold and Integrated DNA Technologies Inc. (1710 Commercial Park Coralville, IA 52241) provided the staple strands and sticky-end strand sequences. The reagents shown in Table 1 are combined to produce a solution consisting of the staple strands, sticky ends, and M13mp18 ssDNA plasmid with a total volume of 150 μL using COB buffer (1X Tris-acetate-EDTA (TAE) buffer with 12.5 mM of MgCl_2).

Table 1. Reagent list for CO-01 0-D with modified sites for biotin

Work	Volume	Final
COB 10X	15 μL	1X
S1, 500 nM	30 μL	100 nM
S6, 1000 nM	15 μL	100 nM
m13mp18, 418 nM	7.2 μL	20 nM
CO-01 L \rightarrow CO-3970 R, 1000 nM	30 μL	200 nM
CO-01 R \rightarrow CO-3970 L, 1000 nM	30 μL	200 nM
HOH	22.8 μL	-----
FINAL TOTAL VOLUME	150 μL	-----

Lists components for an example synthesis. Each entry in the table can be calculated and modified for different types of monomers and sticky ends and terminating ends. The volume of each component can be calculated by multiplying the final concentration by the final volume and then dividing the total by the working concentration. Staples are added in excess to prevent selective connection between successfully folded origami motifs²⁷. S1 and S6 are further described in the appendix.

Depending on whether the solution is supposed to be CO-01 or CO-3970, the appropriate staple strands and sticky ends are included in the anneal mixture. The final concentration of the ssDNA plasmid in the solution is set to 20 nM with the molar ratio of the ssDNA plasmid to each of the other staples being 1:5. The final solution is split into three 50 μL volumes and annealed in

a slow cooling process from 90 to 20 °C over a 10 h period. When using the NanoDrop 1000 3.8.1 both DNA 50 and DNA 33 are options for analysis. DNA 50 is double stranded DNA while DNA 33 is single stranded DNA. Since DNA 33 is the desired values for ss-DNA information, this produces an absorbance value at 260 nm and provides the concentration in ng/ μ L.

NanoDrop Analysis

UV-Vis spectroscopy was performed, using a NanoDrop ND-1000 spectrometer to determine the concentration of a sample and therefore quantify stoichiometries. The NanoDrop is cleaned using milliQ water and a kimwipe. Using the NanoDrop 1000 3.8.1 application, the nucleic acid setting is selected. Making sure that the sample type is set to DNA-50, two μ L of milliQ water is placed for blanking. To ensure a good base line, spectra of milliQ water is recorded for potential errors in the data. Finally, 2 μ L of sample is placed on the NanoDrop and measured and recorded. Afterwards, 2 μ L of milliQ water is used to rinse the stage.

Mica Substrate Preparation

An AFM Specimen Disc with a 15 mm diameter is used to anchor a PELCO Tabs with a 9 mm outer diameter. After the PELCO Tabs are secured on the AFM Specimen Disc, a PELCO Mica Disc with a 9.9 mm diameter is adhered to the PELCO Tab. Figure 25 illustrates the mica substrate used to support samples for AFM Imaging. Mica is a 2-D crystal that can be cleaved to produce a clean surface for new samples. A piece of scotch tape is spread across the mica surface and peeled off to reveal a new fresh mica surface.

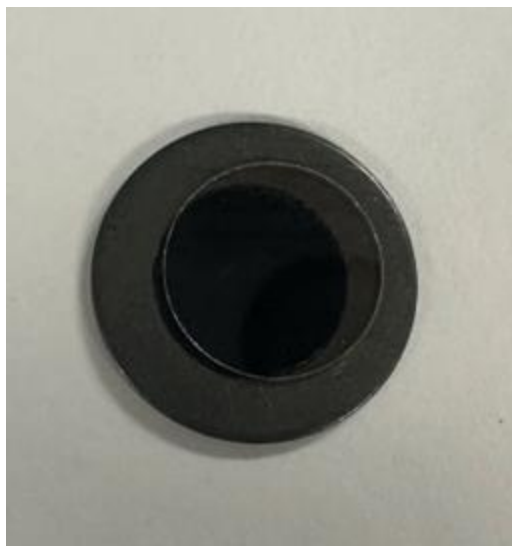


Figure 25. Mica Substrate. Image of a PELCO mica disc secured to an AFM specimen disc utilizing the PELCO adhesive tabs.

Mica Substrate Deposition

The Norton lab has determined that 6 hours is sufficient annealing time if we dwell for longer periods within the active temperature ranges. After the thermal anneal program, 10 μL of the solution is pipetted onto a newly peeled mica substrate. The CO is deposited onto the mica slide and allowed to adsorb for 30 seconds to 5 minutes in a simple humidity chamber, illustrated in Figure 26. The humidity chamber is to prevent the evaporation of the sample once deposited on the mica substrate. Since the product solution deposits on the mica slide for 30 seconds to 5 minutes with only 10 μL , the volume would evaporate outside a simple humidity chamber. Afterwards, the origami droplet is gently wicked off with a kim-wipe, rinsed with Milli-Q water, and dried gently with argon gas flow. For reasonable dispersion/packing of individual structures, the application of origami to mica substrate at concentration of approximately 1 nM or less is applied. The volume must be sufficient to cover the center of the mica surface and to not evaporate during deposition time. It is then ready for AFM imaging.

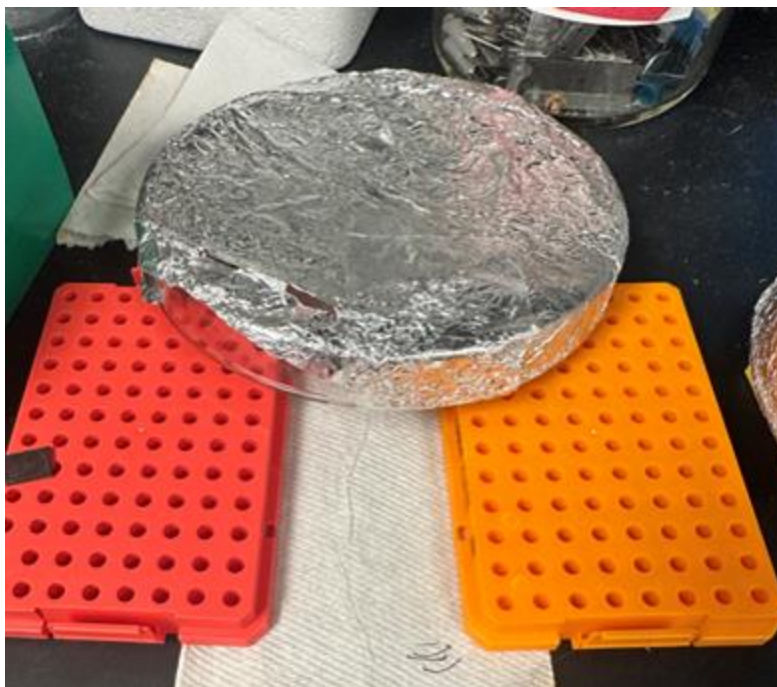


Figure 26. Simple Humidity Chamber. Image of the simple humidity chamber. Recycling two used pipette tip holders and a glass petri dish, the paper towel below is sprayed with water to create moisture for the humidity chamber. For this to work more effectively, the dish could be on the paper towel, if lifted off as shown here, humidity will tend toward ambient.

AFM Imaging

Samples are imaged using a Bruker Multimode 8 AFM, depicted in Figure 27. Before the metal disc with sample is placed in the Bruker Multimode 8 (MM8) AFM, the stage is lowered below the two ball bearings supporting the probe holder to avoid collision of the tip with the sample. Once the stage is lowered, the metal disc with sample is placed on the stage with tweezers. The probe holder is then placed and secured by the clamp. Using the Nanoscope 8.15 application, the scanasyst-air mode, peakforce tapping, is selected. Peakforce tapping is a non-resonant, 2000 Hz tapping imaging mode utilizing a silicon nitride cantilever with a silicon tip having a nominal radius of about 2 nm. The optical portion of the microscope is focused on the surface of the sample. Afterwards, the tip is lowered via the motor control switch. To make sure that the tip is properly aligned and receiving signal, the signal sum display is checked to make

sure that the SUM and VERT/HORZ are within the given values. The SUM_value needs to be above 5 and the VERT/HORZ values need to be zero. Once the parameters of the microscope are set, using the Nanoscope 8.15 program, the parameters are adjusted based on the sample to be imaged. Typically, the parameters are x-y scans of 5 μm , 1.7 μm , and 10 μm with X and Y offsets initially set to 0 and a scan rate of 1 Hz.

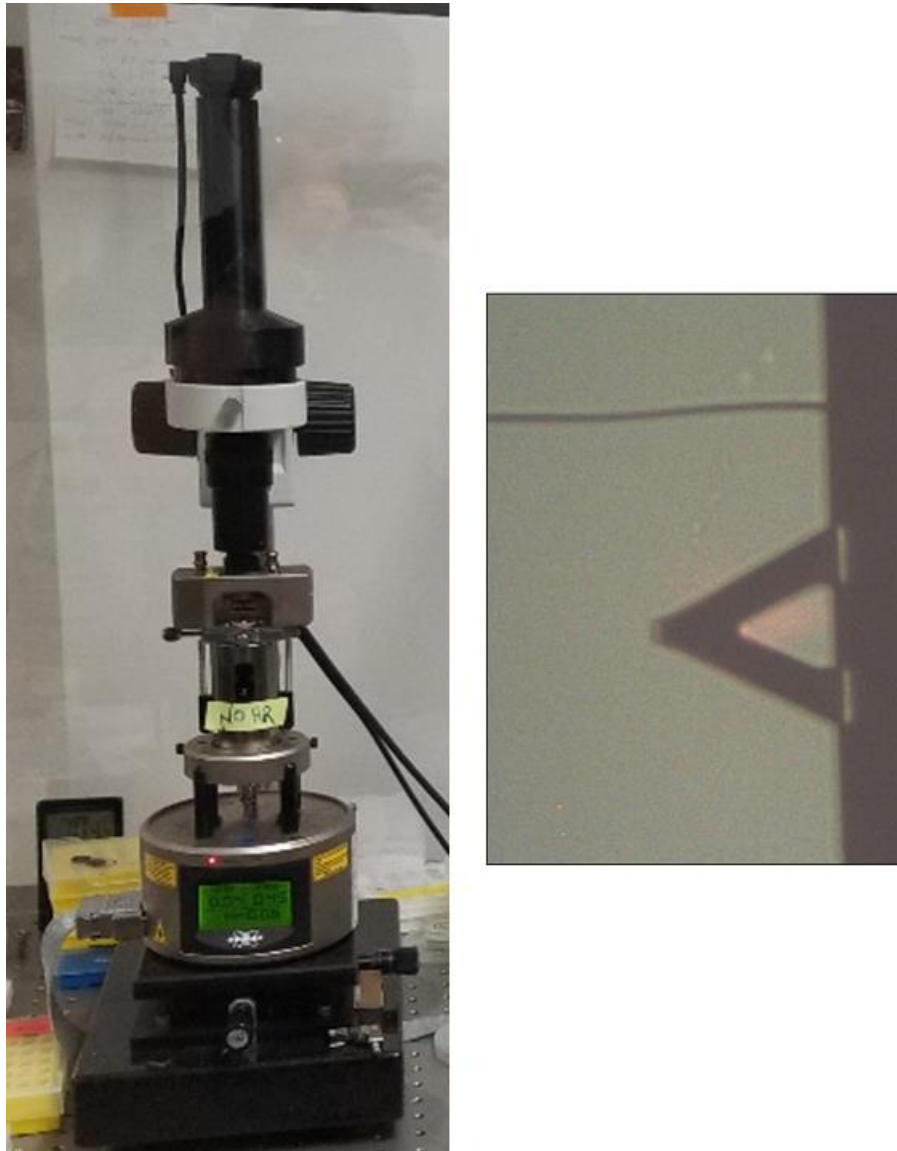


Figure 27. Bruker Multimode 8 and Cantilever. Image of the Bruker Multimode 8 AFM and an optical image of the MM8 cantilever in focus on a mica sample.

Streptavidin (SA) Decoration

There are two protocols for streptavidin (SA) decoration. The first protocol is on surface decoration where 5 μ L of 500 nM SA in COB and 5 μ L of COB 1X are pipetted onto parafilm, mixed, then deposited onto the sample coated the mica substrate for 10 minutes. The second protocol is an in-solution decoration where 5 μ L of 500 nM SA and 5 μ L of COB 1X are pipetted into a 0.2 mL polymerase chain reaction (PCR) tube, after the thermal annealing program, for 10 minutes at room temperature. The volume of origami added was 10 μ L at 10 nM

Thermal Anneal Programs and Time Variations for 1-D Array Growth

During the initial experiments testing 1-D formation, varying thermal anneal programs and times were tested to see if arrays could be formed outside of the standard 50° to 6 °C ramped thermal anneal. Addressing the thermal anneal programs, three different temperatures were tested, room temperature, isothermal at 50 °C, and the standard 50° to 6 °C ramp. After imaging numerous samples prepared with each thermal anneal program, no better thermal anneal program was identified. The next parameter tested was the length of time for thermal anneal program. 5 minutes, 15 minutes, 30 minutes, 1 hour, 3 hours, 5 hours, and overnight were studied. Again, there was no optimal time since the formation of arrays seems to start as soon as the two different types of origami are placed in a PCR tube and seems to proceed quickly. Since both the varying thermal anneal programs and times did not yield a more efficient protocol, the standard thermal anneal program of 50° to 6 °C ramp for 10 hours was utilized from this point forward. Equal parts of CO-01 and CO-3970 are mixed and annealed in the thermal anneal ramp program from 50° to 6 °C for the formation of the dimer building blocks, 1D, and 2D arrays. Depending

on whether the sample is a dimer building block, 1D, or 2D array, the designed monomer will have terminating ends or specific sticky ends to connect to the other monomer.

Nucleated Growth Through Titration

Array growth through successive addition is illustrated in Figure 28. A terminated CO-01 was mixed with equal parts CO-3970 to create a dimer “building-block”. Then a stoichiometric amount of CO-01 was added to this dimer and annealed to create a trimer. Another stoichiometric aliquot of CO-3970 was added to this trimer and annealed to create a 4-mer. This pattern was repeated until the desired 8-mer was created.

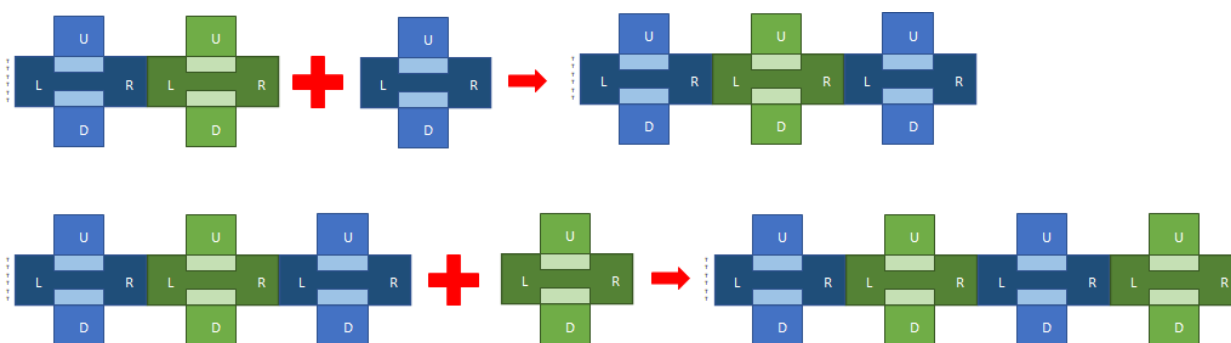


Figure 28. Nucleated Growth Through Titration. Illustration of the nucleated growth through titration process. The initial dimer has CO-01 added to create the trimer. The next step would be to add CO-3970 for a 4-mer

Diafiltration

A diafiltration process is used to remove excess staples from an origami product. The Amicon Ultra 0.5 mL centrifugal filter and tube is pretreated with 400 μ L of 1X COB placed in the tube and spun for 5 minutes at 12,000 rpm at 19°C. The step is repeated however, 25 μ L of sample is also added. The time is then modified to 3 minutes and 400 μ L of COB 1X is added and diafiltered. The final step is to invert the filter in the tube and change the spin rate to 3000 rpm and to run it for 3 minutes to collect the product.

Gel Electrophoresis

A mini-horizontal unit electrophoresis apparatus and gel box are soaked in soapy water overnight. The apparatus and box are rinsed using DI Water. Using 99% glycerol as lubricant and the rubber gasket edging, the gel box is lubed and placed into the electrophoresis apparatus. Depending on the strength of the gel, a different mass of Megabase Agarose (1000 Alfred Nobel Drive Hercules, CA 94547) is measured and added to 70 mL of the buffer solution in a 250 mL Erlenmeyer flask (e.g., 1% gel strength requires 0.7 g of Megabase Agarose). Using a microwave oven, the solution is heated (~ 1 – 3 minutes, avoiding boiling) sufficiently to ensure proper dissolution of the agarose into the buffer solution. After the solution is cool to the touch, the solution is poured into the gel box. Again, depending on the sample, the appropriate number and type of gel comb is placed into the gel to make the wells. After approximately 45 minutes, the gel should have set and both the gel box and combs are removed from the electrophoresis apparatus. The gel bed is then rotated 90° and the electrophoresis box is filled with the buffer solution until the buffer solution barely covers (~0.5 cm) the top of the gel. The apparatus is placed in an ice bath and the PowerPac Basic voltage is set to the appropriate values for the samples. Table 2 is an example showing the general guidelines for preparing solutions to be mixed then pipetted into the wells to load the samples.

Table 2. Loading lanes for gels

Lane	DNA Type	DNA Volume (μL)	DNA Concentration (nM)	DNA Mass (ng)	Glycerol Volume (μL)	1x TAE with 12.5 μM MgCl_2 (μL)	Total Volume (μL)
1		4	-----	2000	5	31	40
2		35	20	570	5	0	40
3		35	20	570	5	0	40
4		35	20	579	5	0	40
5		3	-----	-----	0	38	40
6		35	20	570	5	0	40
7		35	20	570	5	0	40
8		35	20	570	5	0	40
9		35	20	570	5	0	40
10		8	-----	-----	5	27	40

Lane 1: 1 kb DNA Extension Ladder

Lane 2-4: Samples at 20 nM

Lane 5: Blue/Orange 6X Dye

Lane 6-9: Samples at 20 nM

Lane 10: High DNA Mass Ladder

After the gel wells are loaded with sample, the gel is run for either 1 or 2 hours and extraction of the sample is conducted using both the UV table and MiniBIS Pro Gel

Documentation (Neve Yamin, Israel).

Gel Analysis

Depending on the sample, 4 different types of equipment are utilized to analyze the sample in the gel. The UVGL-58 Handheld UV Lamp (Analytik Jena) is utilized to help image DNA using the shadowing technique. The stained gel is placed on the gel doc bed and the UCGL-58 Handheld UV Lamp is placed in the gel imager for imaging. The UCGL-58 Handheld

UV Lamp was utilized due to TLC plate being located on the UV bed and preventing the UV bed light from being utilized. Using the GelCapture application, the exposure, gain, and brightness are adjusted to produce and image the visible bands. Visible bands are bands seen through either the MiniBIS Pro UV Gel Doc or through the White/2 UV transilluminator table, where bands with sample are stained with specific fluorescent stains. The second type of equipment is the MiniBIS Pro UV Gel Doc. The MiniBIS Pro UV Gel Doc utilizes either UV or white light to help image the gel. The stained gel is placed onto the appropriate gel bed and the iris and focus are adjusted for imaging. Using the GelCapture application, the exposure, gain, and brightness are adjusted to produce an image with bands. The third type of equipment used is the White/2UV Transilluminator table and Silica G TLC Plates for the shadowing technique. The Silica G TLC plate is wrapped in saran wrap and placed beneath the gel. Using the gel imager, the gel is imaged using the UVGL-58 Handheld UV Lamp.

On-Mica Deposition

A mica slide is cut into triangular shaped pieces that will fit inside the PCR tube. After cutting the mica into the appropriate dimensions, the cut mica is placed in the PCR tube with solution and allowed to deposit for the 1-hour thermal anneal. After the deposition time, the cut mica is removed from the PCR tube, dried with argon gas, rinsed with ddUV water, and dried with argon gas. Finally, the cut mica is secured onto a metal disc with the PELCO tabs for AFM imaging.

On-Glass Deposition

A template for a glass insert in the form of an isosceles trapezoid shape tapered to fit into a PCR tube, measuring 3 mm at the top, 1 mm at the bottom with a taper length of 8 mm and a taper angle of ~ 7 degrees was designed. Using double sided tape, a 12 mm diameter glass

coverslip is secured onto a paper copy of the template design to guide the cutting of the glass. The glass is scribed along the template guiding lines using a diamond scribe, then cracked along the scribed lines. After cutting the glass to the appropriate dimensions, the cut glass is sonicated for 5 minutes in ethanol, sonicated for 5 minutes in acetone, and UV treated for 15 minutes in the UVL-20 apparatus to remove fluorophores. The cleaned cut glass can then be placed in the PCR tube with solution and the origami constructs are allowed to deposit during a 1-hour thermal anneal. After the deposition time, the cut glass is removed from the PCR tube, dried with argon gas, rinsed with ddUV water, and dried with argon gas. Finally, the cut glass is secured onto a metal disc with the PELCO tabs for AFM imaging.

Refined Dendron to Conjugated DNA Synthesis

The process of attaching the refined dendron to conjugated DNA can be broken down into a 5-day procedure, illustrated in Figure 29.

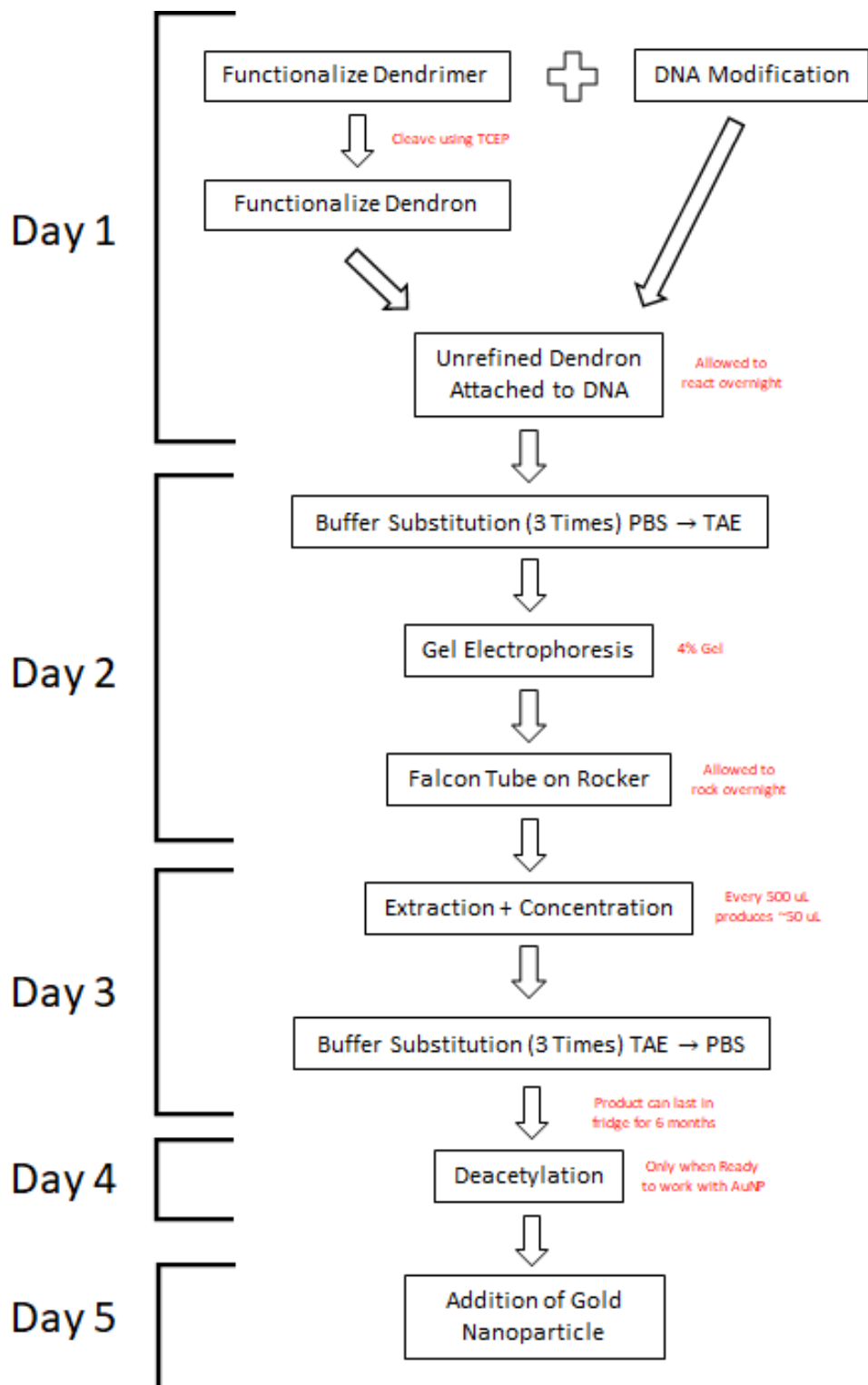


Figure 29. Protocol for Synthesized Conjugates. Schedule and protocol for the synthesis of conjugate to gold nanoparticle.

On day 1, the functionalization of the dendrimer and modification of the DNA are done in tandem. When functionalizing the dendrimer, 0.079 mg of N-succinimidyl-S-acetylthiopropionate (SATP) is dissolved in 20 μ L of DMSO. Dilute the solution with 475 μ L of pH 7.2 phosphate-buffered saline (PBS). Add 5 μ L of 51.37 mM G2 Dendrimer. This is to ensure a 1.25:1 molar ratio of SATP to each primary amine on the periphery of the dendrimer. Allow the reaction to react for 1 hour at room temperature. Using 3000 NMWL cutoff filters, the solution is placed in the centrifuge for 30 minutes at 15000 G. After measuring and disposing of the waste product, equal parts of PBS to sample are added to the filters and diafiltered again for 30 minutes at 15000 G. This step is repeated once more. The 3000 NMWL cutoff filter is inverted and run for 30 minutes at 15000 G to recover the product. The remaining solution should be \sim 50 μ L. For DNA modification, dissolve 1.494 mg of sulfosuccinimidyl 4-(N-maleimidomethyl)cyclohexane-1-carboxylate (SSMCC) in 20 μ L of dimethyl sulfoxide (DMSO). Dilute the solution with 480 μ L of pH 7.2 PBS. Add 1.7 μ L of 100 mM DNA. This is to ensure a 2:1 molar ratio of sulfo-SMCC to ssDNA. Allow the reagents to react for 1 hour at room temperature. Using 3000 NMWL cutoff filters, the solution is placed in the centrifuge for 30 minutes at 15000 G. After measuring and disposing the waste product, equal parts of PBS and sample are added to the cutoff filter and diafiltered again for 30 minutes at 15000 G. This step is repeated once more. The 3000 NMWL cutoff filter is inverted and run for 30 minutes at 15000 G to recover the product. The remaining solution should be \sim 50 μ L. After both reactions have been completed, the dendrimer is functionalized into a dendron. This is when 1.319 mg of tris(2-carboxyethyl)phosphine (TCEP) is added to the \sim 50 μ L of functionalized dendrimer. This is to ensure a 2:1 molar ratio of TCEP to each dendrimer for the cleaving. Allow the reaction to proceed for 1 hour at room temperature. Finally, the unrefined dendron is attached to the

modified DNA. Equal parts of the functionalized dendron and modified DNA are added to a tube to yield roughly 100 μ L as the final volume and allowed to react overnight at room temperature.^{28,29}

The second day a buffer substitution is run. Depending on how much sample is retrieved from day 1, x μ L of tris-acetate-EDTA (TAE) is added to the solution to yield a total volume of 500 μ L. The solution is then diafiltered for 7 minutes at 15000 G in a 10000 NMWL cutoff filter. The diafiltration process is repeated 2 more times. Finally, the 10000 NMWL cutoff filters are inverted and run for a final 7 minutes at 15000 G. Gel electrophoresis is performed as part of a purification process. The gel bed is lined with rubber lining and lubricated using 99% glycerol and placed in the gel apparatus at a 90° angle. 2.4 g of Agarose is placed in an Erlenmeyer flask with 70 mL of 1X TAE and 7 μ L of 10000X Ethidium Bromide (EtBr). The mixture is placed in a microwave and heated until the solution bubbles. The solution is left to cool to touch and poured into the gel setting apparatus. After the gel has solidified, the gel bed is removed along with the rubber lining. The gel bed is rotated another 90°. Using the table, the wells are filled with samples. The gel apparatus is filled with 1X TAE until it just covers the top of the gel. It is then run for 30 minutes at 150 V. The gel is then imaged on the gel doc and taken to the UV Vis table for band extraction. The desired bands are then extracted and cut into small cubes. The cubes are then placed in a falcon tube filled with TAE just barely covering the gel product. On a rocker, the solution is allowed to extract overnight at room temperature.

Before day 3 is conducted, the solution is stable for up to 6 months in a refrigerator. On day 3, a final buffer substitution is conducted. 200 μ L of sample is added to 300 μ L of ddUV water and diafiltered for 7 minutes at 15000 G in a 10000 NMWL cut off filter. The same step is

repeated 2 more times. Finally, the 10000 NMWL cutoff filter is inverted and runs for 7 minutes at 15000 G.

On day 4, the total volume of the solution is brought up to 200 μL and 10 μL of Hydroxylamine is added to create at least a 2:1 molar ratio with each functionalized primary amine of the conjugates in the tube containing the conjugate solution. 10 μL of TCEP is added to create a reducing environment in the solution to attempt prevention of any and all future possible disulfide bonds forming among and within conjugates after the deprotection of the sulfhydryls. Since resin is delivered suspended in a TE (Tris EDTA) buffer, 250 μL of ddUV water is used to resuspend the resin in the G-50 column. The specific resin is Sephadex G-50 DNA Grade, which is pre-equilibrated in TE buffer with 0.05% KathonTM CG/ICP biocide. The resin itself acts as the medium of purification that allows the rapid purification of DNA from unincorporated labeled nucleotides. Since the resin is in a TE buffer, when purchased, water is substituted/resuspended in the resin instead of TE buffer. The column is then placed in the supplied collection tube and spun for 1 minute at 3000 G. Add 250 μL of sample and spin for 2 minutes at 3000 G. This is repeated till all the solution has been filtered. 40 nm AuNP are concentrated and added to the refined conjugates in a 5:1 molar ratio and left at room temperature overnight.

On day 5, the AuNP conjugate is added to CO-01 in a 5:1 molar ratio and left to react overnight at room temperature.

CHAPTER 7

RESULTS AND DISCUSSION

Thermal Anneals

The initial experiments were performed to compare the variables of time and temperature as those are independent variables for the assembly of the dependent variable of the length of infinite alternating 1-D arrays. Figure 30 shows the three different types of thermal anneal programs used to test whether time or temperature was crucial to determining infinite 1-D alternating array length.

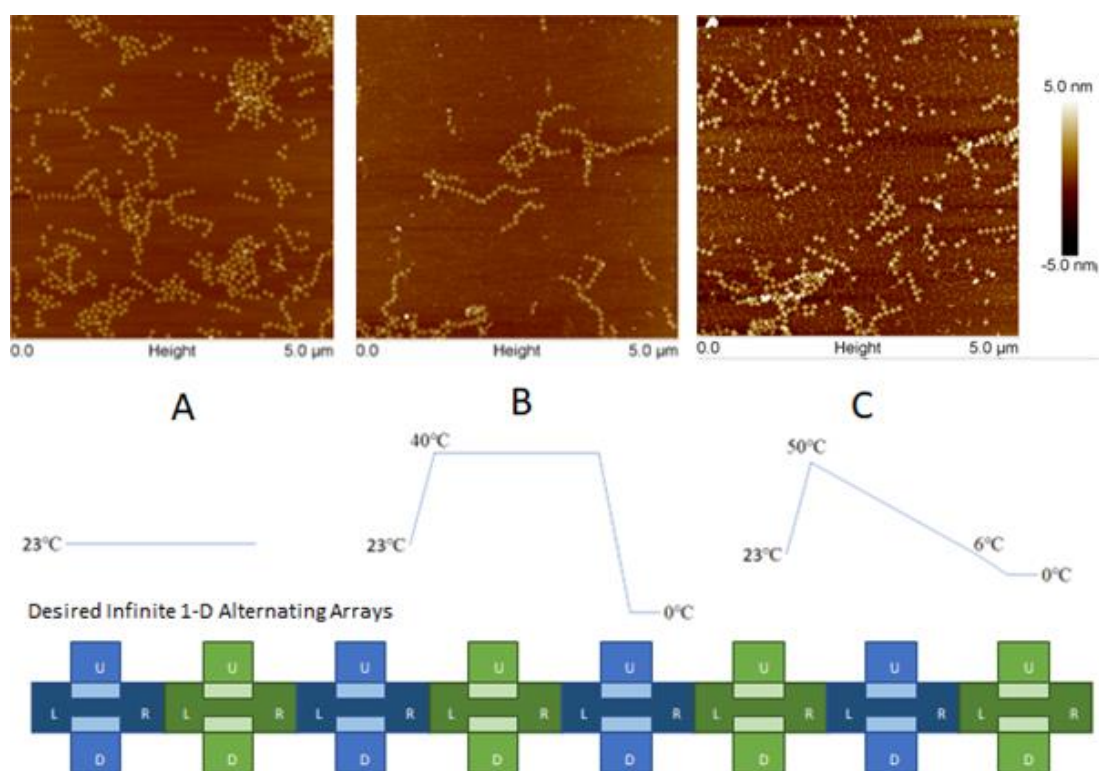


Figure 30. Thermal Anneal Program Comparison. Top) AFM images indicating the relative length of the 1-D alternating arrays formed by manipulating both time and temperature. Middle) Thermo-Temporal programs: Figure 30 A represents a room temperature anneal program lasting for 1 hour. Figure 30 B represents an isothermal temperature anneal at 40°C for 1 hour. Figure 30 C represents the Tsai Chin thermal anneal program which requires 12 hours. Bottom) Illustration of designed infinite 1-D alternating arrays.

In Figure 30 A, both time and temperature were reduced to see if a 1-hour room temperature anneal program would work. As one can see, the formation of 1-D alternating arrays did occur, but the length of the arrays should be much greater since the solution is comprised with “infinite” components. Figure 30 B shows an isothermal anneal program of 40°C for 1 hour, where 1-D alternating arrays form, but with longer arrays than the room temperature anneal program. Figure 30 C depicts the Tsai Chin Wu et al.³ thermal anneal program, where 1-D alternating arrays length is maximized with both time and temperature. As one can see in Figure 30 C, infinite alternating arrays with longer array lengths were produced. With more time added to the thermal anneal program, the temperature ramp needed can be removed to produce longer arrays. Since time can produce longer arrays without the need for thermal anneal programs, Tsai Chin Wu et al.³ thermal anneal program was conducted again to confirm that time was the independent variable that determined the length of 1-D alternating arrays.

In another aspect of our work, the original goal was to create dimers with CO-01 T and CO-3970 at room temperature. The assembled dimer would serve as the “initiator” to the 1-D array leading to the assembly of finite alternating 1-D arrays, by titration, to grow the arrays one monomer at a time. However, looking at Figure 31, it was assessed that temperature did not directly impact the yield of dimers formed.

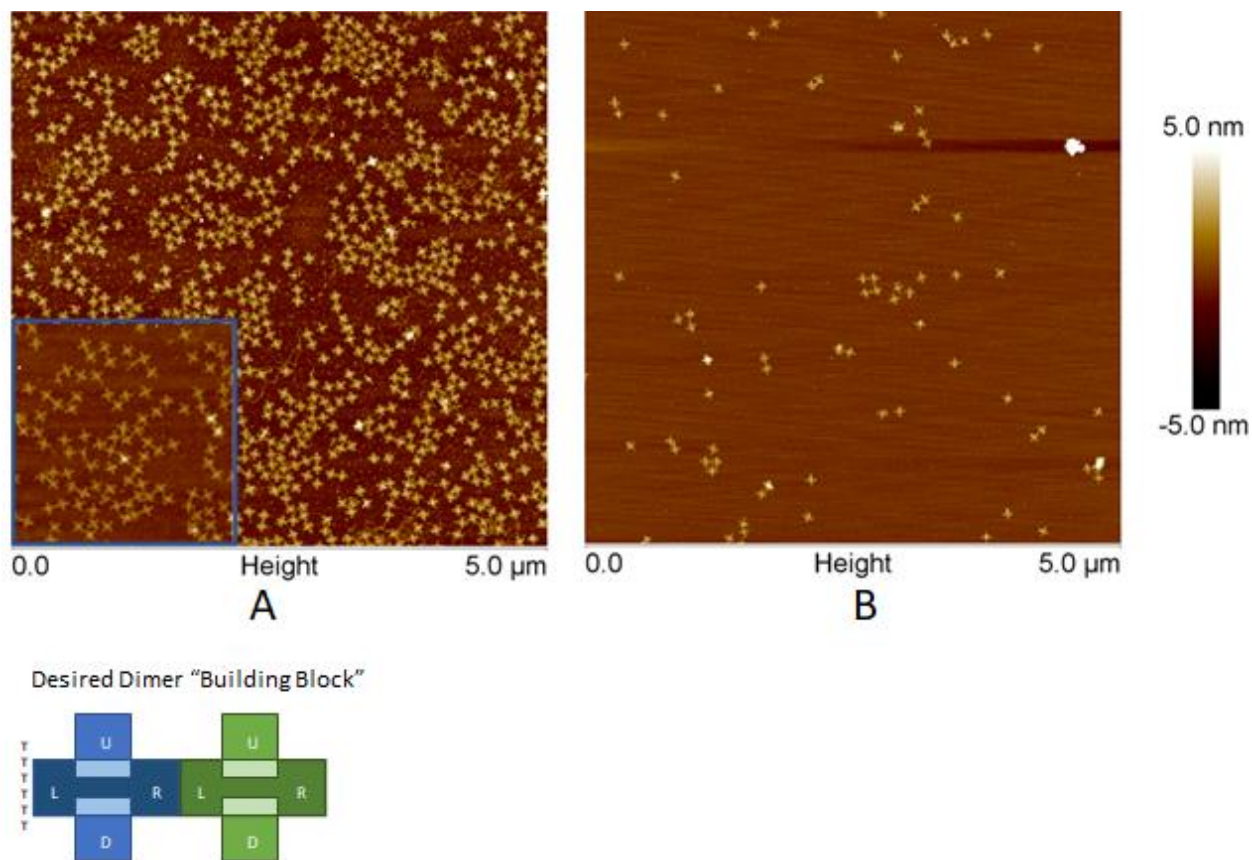


Figure 31. CO-01 T and CO-3970 with SA. AFM images of products of reaction of CO-01 T and CO-3970 with SA mixed in equal parts to synthesize dimers. Figure 31 A depicts formation of dimers at room temperature for 30 minutes. Figure 31 B depicts formation of dimers using a temperature program ramp from 45°C to 6°C over 24 hours.

The intended purpose of a room temperature anneals for 30 minutes, shown in Figure 31 A, was to push the thermal anneal program to an extreme. By removing both temperature and time utilized in the Tsai Chin Wu et al.³ programs, the experiment should reflect what happens to CO when both temperature and time are reduced. This resulted in a lack of dimers produced with many monomers still present in the AFM image. To make sure that the dimers were not just misassembling, Tsai Chin et al.³ thermal anneal program was conducted, in Figure 31 B the intended purpose of a thermal anneal program of 45°C to 6°C for 24 hours is to determine what happens to CO when both temperature and time are increased. Since both temperature and time are maximized, the number of dimers to monomers present is skewed towards dimers being the

predominant product formed. Although the results proved that dimers do assemble at higher yields with extended time and higher temp, the amount of time and the temperature ramp can be modified to be more efficient. To confirm this hypothesis, the idea of assembling infinite 1-D arrays following the two different anneal programs were conducted to determine if the different temperature and time would impact the length of the arrays.

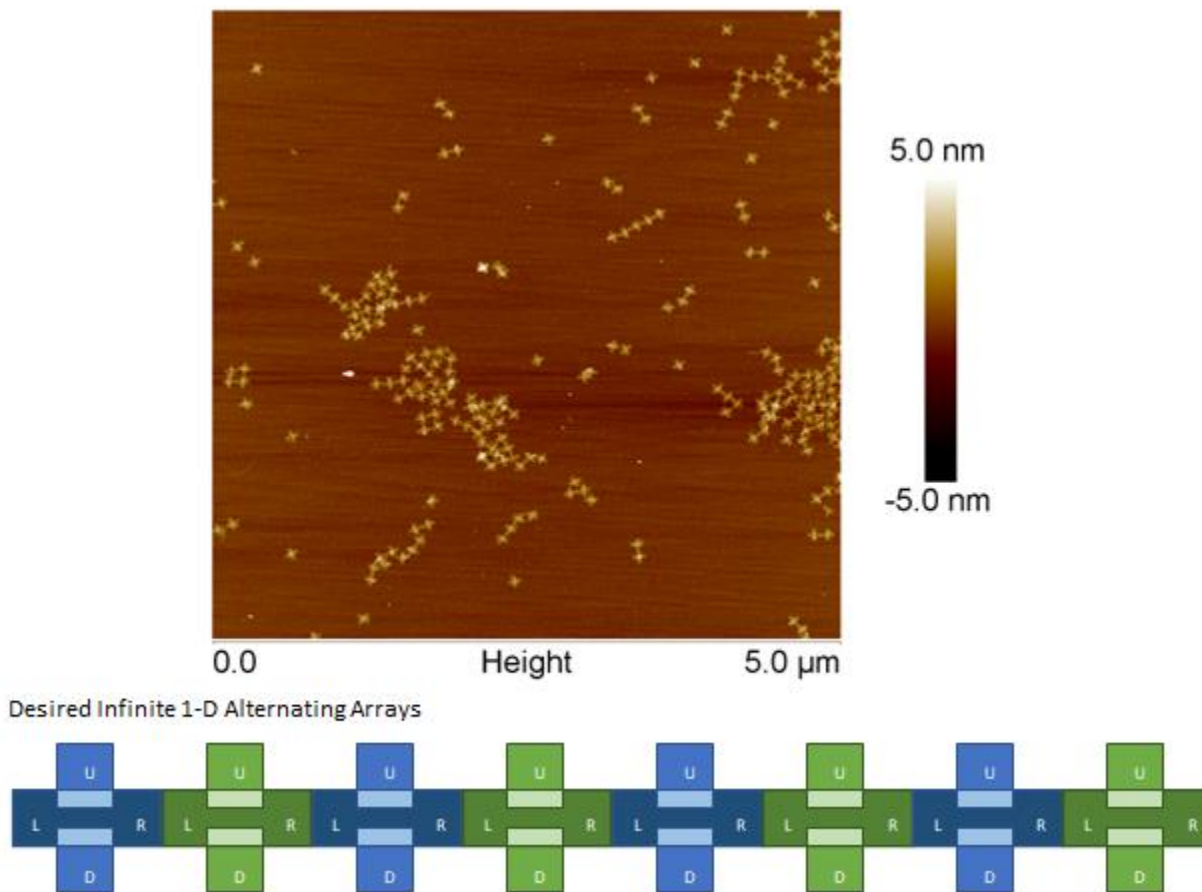


Figure 32. CO-01 with MBv2 and CO-3970 with Thermal Program of 45°C to 6°C for 24 Hours. AFM image of the products obtained when pre-formed CO-01 MBv2 and CO-3970 are mixed with equal quantities in a tube and allowed to form infinite 1-D arrays in the thermocycler using a temperature program of 45°C to 6°C for 24 hours.

Figure 32 shows the results when both time and temperature were maximized to create infinite arrays. Since this program follows Tsai Chin et al.³ thermal anneal program, our lab considers this the “gold standard” for 1-D infinite array assembly.

3 Base Pair (BP) Sticky Ends (SE) vs 5 BP SE

A set of 3 BP SE vs 5 BP SE experiments was conducted to test the length of arrays produced using two different lengths of SE. In Figure 33 A, 3 BP SE show that 1-D alternating arrays are formed; however, the length of the 1-D alternating arrays observed were not as long as would be expected under “infinite” solution conditions. Since 3 BP SE were not potent enough to create the infinite 1-D alternating arrays sought, 5 BP SE were utilized for the rest of the experiments. In Figure 33 B, the 5 BP SE CO were shown to provide longer 1-D alternating “infinite” arrays compared to the 3 BP SE through AFM analysis. Since the 5 BP SE were much more effective creating the 1-D alternating arrays, 5 BP SEs were used in all the future work and designs.

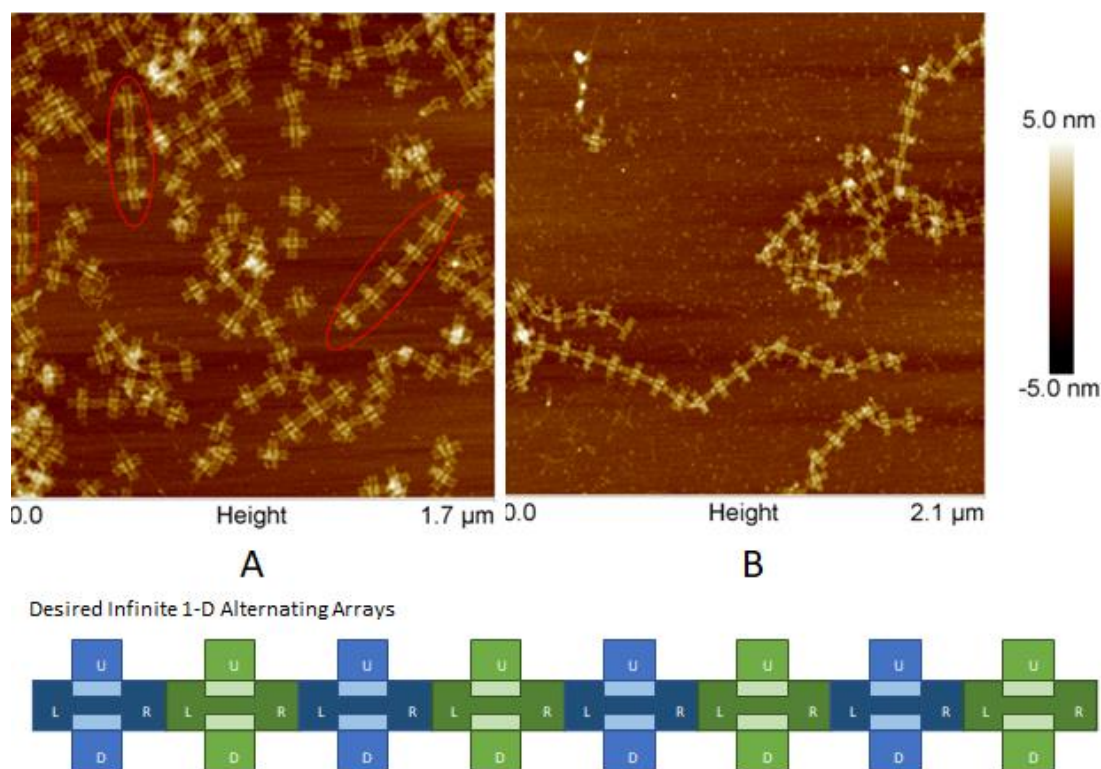


Figure 33. 3 BP SE vs 5 BP SE. AFM images which contrast the difference in length of the 1-D alternating arrays. Figure 33 A depicts the 3 BP SE where the longest 1-D alternating array in the AFM image is a 6-mer. Figure 33 B depicts the 5 BP SE where the longest 1-D alternating array in the AFM is a 19-mer.

Stoichiometry

Since it is difficult to get a perfect 1:1 ratio of two monomers, due to mechanical and user error based limitations in pipetting, the experiment was conducted by making different ratio of the monomers mixed in an 8 μL volume, diluted to a final volume of 20 μL with COB 1X, and labeled with a mixture of 5 μL of 500 nM SA and 5 μL of COB 1X. AFM images of the resulting materials are shown in Figure 34.

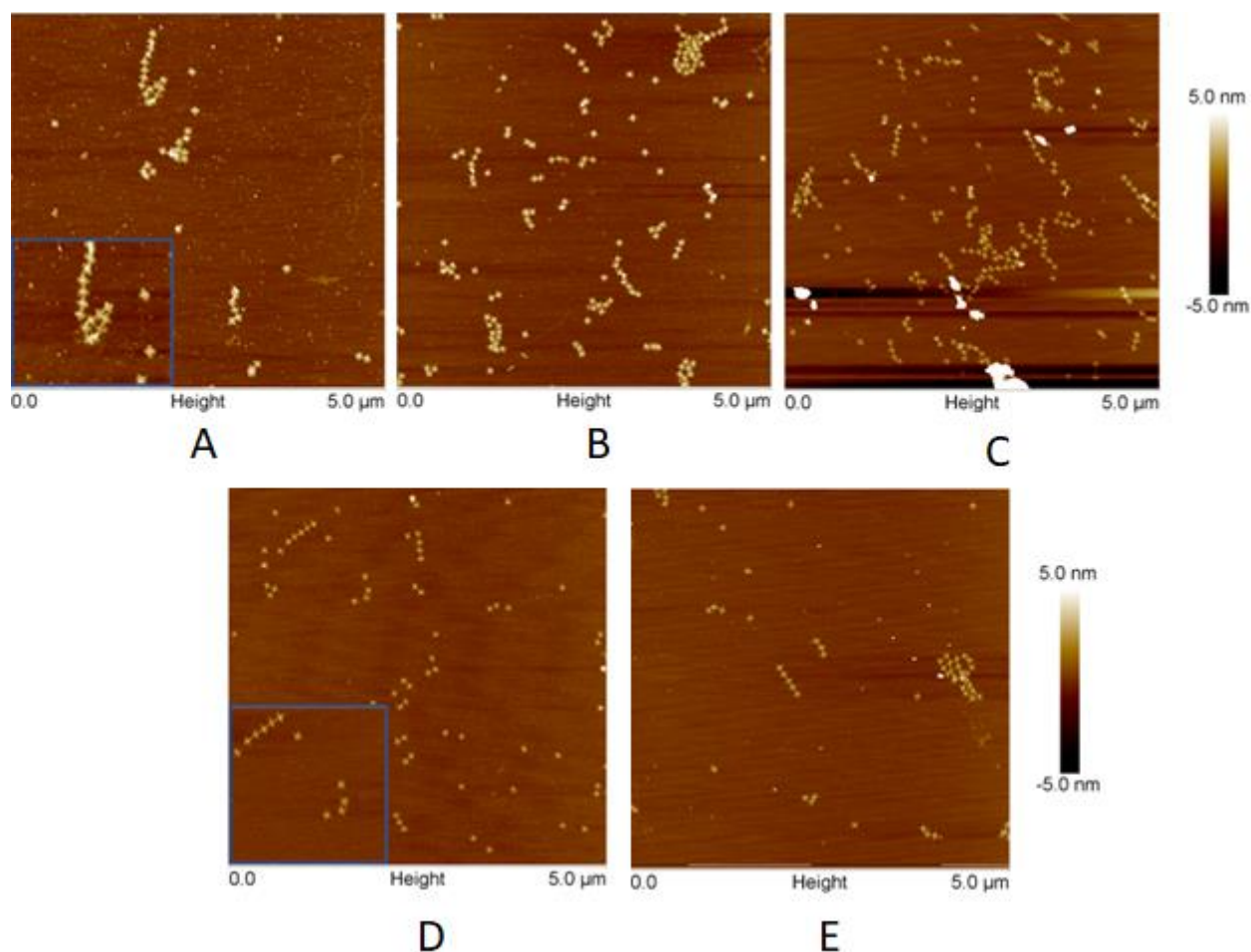


Figure 34. Stoichiometric Experiments. Example AFM images illustrating that the length of the 1-D alternating arrays is dependent on the ratio of CO-01 to CO-3970. Figure 34 A depicts a 4:1 CO-01 to CO-3970. Figure 34 B depicts a 2:1 CO-01 to CO-3970. Figure 34 C depicts a 1:1 CO-01 to CO-3970. Figure 34 D depicts 1:2 CO-01 to CO-3970. Figure 34 E depicts 1:4 CO-01 to CO-3970. Further analysis is in Appendix E.

In Figure 34 A, a 4:1 CO-01 to CO-3970 ratio was conducted, this was to test if saturating the solution with CO-01 would shorten the lengths of the alternating 1-D arrays. However, the arrays did not shorten as indicated in the zoomed portion of Figure 33 A. To make sure that the arrays were saturated with CO-01, the CO-01 was modified with biotin related staples to have SA show on the left and right arms. After doing a close analysis, it was shown that there were more CO-01 than CO-3970 on the substrate. In Figure 34 B, a 2:1 CO-01 to CO-3970 was conducted to again shorten the length of the alternating 1-D arrays. As shown in Figure 31 B, the length of the alternating arrays was shortened with respect to a 1:1 ratio. Again, SA was used to label CO-01 and after analysis, there were more unbound CO-01 than CO-3970 present on the substrate. In Figure 34 C, a 1:1 CO-01 to CO-3970 experiment was conducted to create the infinite alternating 1-D arrays. As depicted in Figure 32 C, the lengths of the alternating arrays are quite long. Using SA to label CO-01, it was analyzed and shown that CO-01 and CO-3970 were in equal numbers in the AFM image. In Figure 34 D, a 1:2 CO-01 to CO-3970 was conducted to manipulate the lengths of the alternating 1-D arrays. Using SA to identify the CO-01, the arrays were shortened with CO-3970 being excess in the arrays. In Figure 34 E, a 1:4 CO-01 to CO-3970 was conducted to manipulate the lengths of the alternating 1-D arrays. Using SA to identify the CO-01, the arrays were shortened with excess CO-3970 being on the substrate. In Figures 34 A through E, the stoichiometric ratio of the CO-01 Biotin and CO-3970 were manipulated to assemble short (monomers to 3-mers), medium (3-mers to 5-mers), and long/infinite arrays (5-mers to infinite). These results are summarized in Table 3. It can be noted that there is a correlation between stoichiometry and the length of 1-D linear arrays. That is, the yield of 5-mers and 6-mers is maximized at the 1:1 ratio.

Table 3. Monomer count for each variation in stoichiometric experiments.

Monomer Count	4:1	2:1	1:1	1:2	1:4
Monomer with SA	11	15	11	11	1
Monomer no SA	2	8	14	11	9
Dimer	2	10	8	16	2
3-mer	3	6	24	3	9
4-mer	20	4	0	4	0
5-mer	0	5	15	5	5
6-mer	0	0	6	0	0
Unidentifiable	18	113	85	28	29
Total	56	161	162	78	55

Nucleated Growth and Successive Addition

In one set of experiments, nucleated growth through successive addition was conducted without diafiltration steps. Since the “one-pot” synthesis of self-assembly of the desired 8-mer 1-D alternating arrays had flaws, a nucleated growth from a terminated dimer was implemented. As illustrated in Figure 35, first, a CO-01 T and CO-3970 were assembled into a dimer. Next, CO-01 was added to create a trimer. The pattern was repeated through 4 cycles to attempt the growth of the desired 8-mer.

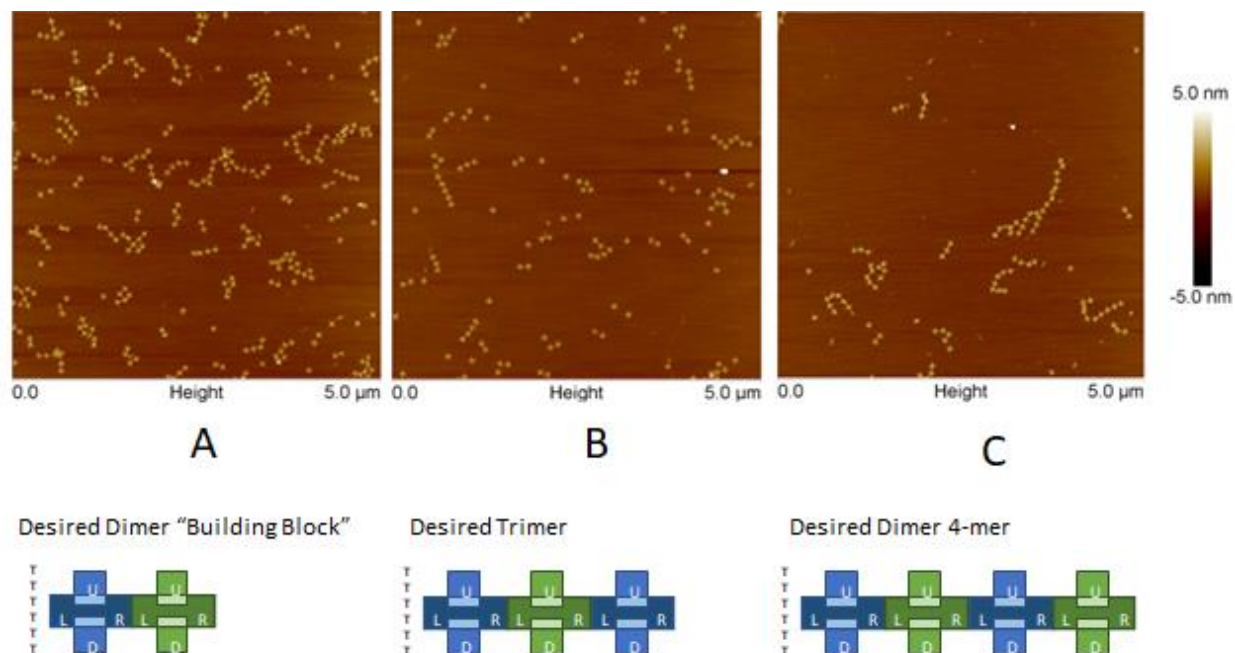


Figure 35. Nucleated Growth Through Successive Addition. AFM images associated with the controlled growth of a dimer “building block” into a 4-mer through successive addition of CO-01 and CO-3970. Figure 35 A depicts CO-01 T and CO-3970 to create a dimer “building block”. Figure 35 B depicts the dimer “building block” with the addition of CO-01 to create a trimer. Figure 35 C depicts the trimer with the addition of CO-3970 to create a 4-mer.

As depicted in Figure 35 A, CO-01 T and CO-3970 were annealed to assemble dimers. This was conducted as the base “building block” for the desired 8-mer product after a series of CO-01 and CO-3970 successive additions. Figure 35 B depicts the trimers formed after adding CO-01 to the dimer building block from the prior step. As shown in Figure 35 B, trimers were formed; however, there was a significant amount of by-product formed, monomers and dimers. Since trimers were present, the next step of adding CO-3970 was conducted. Figure 35 C depicts the 4-mer product created using the 3-mer product and adding CO-3970 to the solution. However, after creating the 4-mer product, the product was contaminated with dimers, trimers, and excess monomers. Since the solutions of each CO has an excess of SE, the hypothesis was that the excess SE inhibited product formation. Thus, diafiltration was introduced to reduce the amount of SE in the solution to reduce the overall amount of incomplete products.

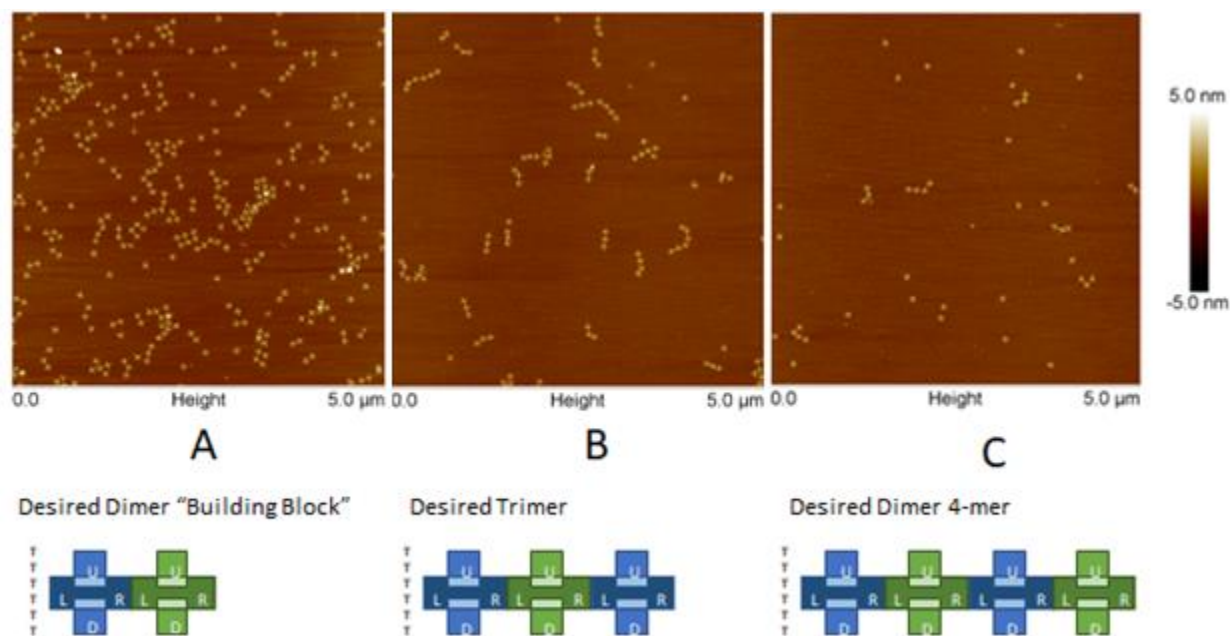


Figure 36. Diafiltered Nucleated Growth Through Successive Addition. AFM images of steps in the controlled growth of a diafiltered dimer “building block” into a diafiltered 4-mer through successive addition of CO-01 and CO-3970. Figure 36 A depicts CO-01 T and CO-3970 to create a dimer “building block” and then diafiltered. Figure 36 B depicts the dimer “building block” with the addition of CO-01 to create a trimer which was then diafiltered. Figure 36 C depicts the trimer with the addition of CO-3970 to create a 4-mer which was then diafiltered.

Figure 36 A depicts the diafiltered product of combining CO-01T and CO-3970 to create the dimer building block for successive addition. Although there were high amounts of dimers produced, some monomers were present as incomplete products. The experiment was continued and CO-01 was added in succession. Figure 36 B depicts successive addition of CO-01 to the dimer building block to create trimers. Although there are a fair number of isolated trimers present in the AFM image, there are still many monomer and dimer products. Since, the solution has been diafiltered of the excess SE, the further addition of CO-3970 to the “trimer” solution was performed. Figure 36 C depicts products of this subsequent addition of CO-3970 to the trimer product to create 4-mers. As shown in Figure 36 C, there was only one 4-mer produced/imaged. Although the diafiltration process seemed to reduce the amount of truncated product formed at the trimer stage, the amount of desired 4-mer product was also reduced. Since

diafiltration did not produce acceptable yields (~ at least 50%), the idea of using gel electrophoresis to purify lengthened arrays was investigated.

Gel Purification

Optimizing the gel purification process can be broken down into 3 sections entailing the determination of the optimal stain, shadowing, and UV-table guided extraction. Since there are different types of stains used to identify DNA in gels, choosing the most optimal stain was conducted. The three types of stains used were ethidium bromide (EtBr), Sybr Green, and Sybr Gold. Figure 37 demonstrates that Sybr Gold was the best candidate for this application due to its relative brightness and therefore its ability to make weak bands relatively more visible.

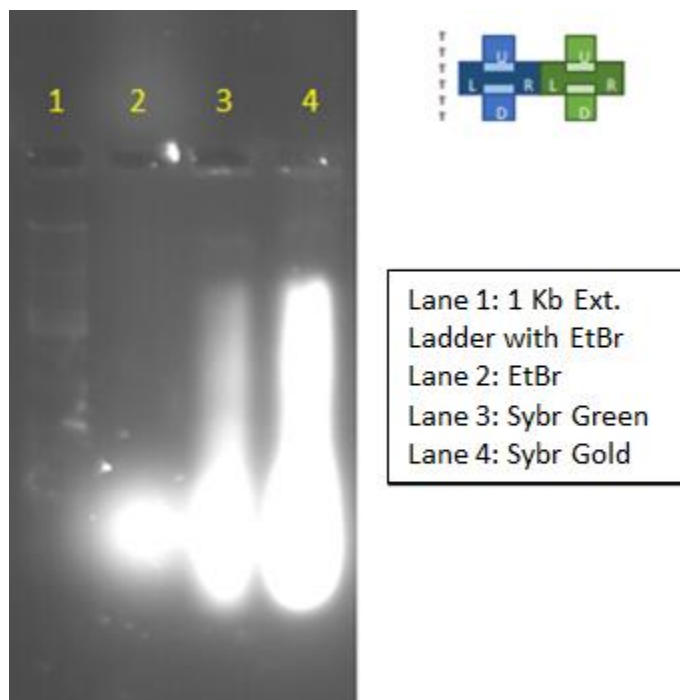


Figure 37. Gel Image of 3 Different Stains Using Dimer Sample. Gel image illustrating the relative intensity of three different stains using a dimer sample.

Although Sybr Gold had a high background, the intensity of the stain was more important for gel extraction.

The second important aspect of gel purification was shadowing. Initially, the project was focused on using MBv2 as the modifier on the CO for super resolution imaging. Since MBv2 is a fluorophore, the stains used in the previous experiment would interfere with the fluorescence of the MBv2. Thus, the shadowing technique was implemented to bypass the removal of the staining process. Figure 38 shows that the shadowing technique worked with smaller structures such as the monomer band, but the dimer bands and larger structures were difficult to identify.

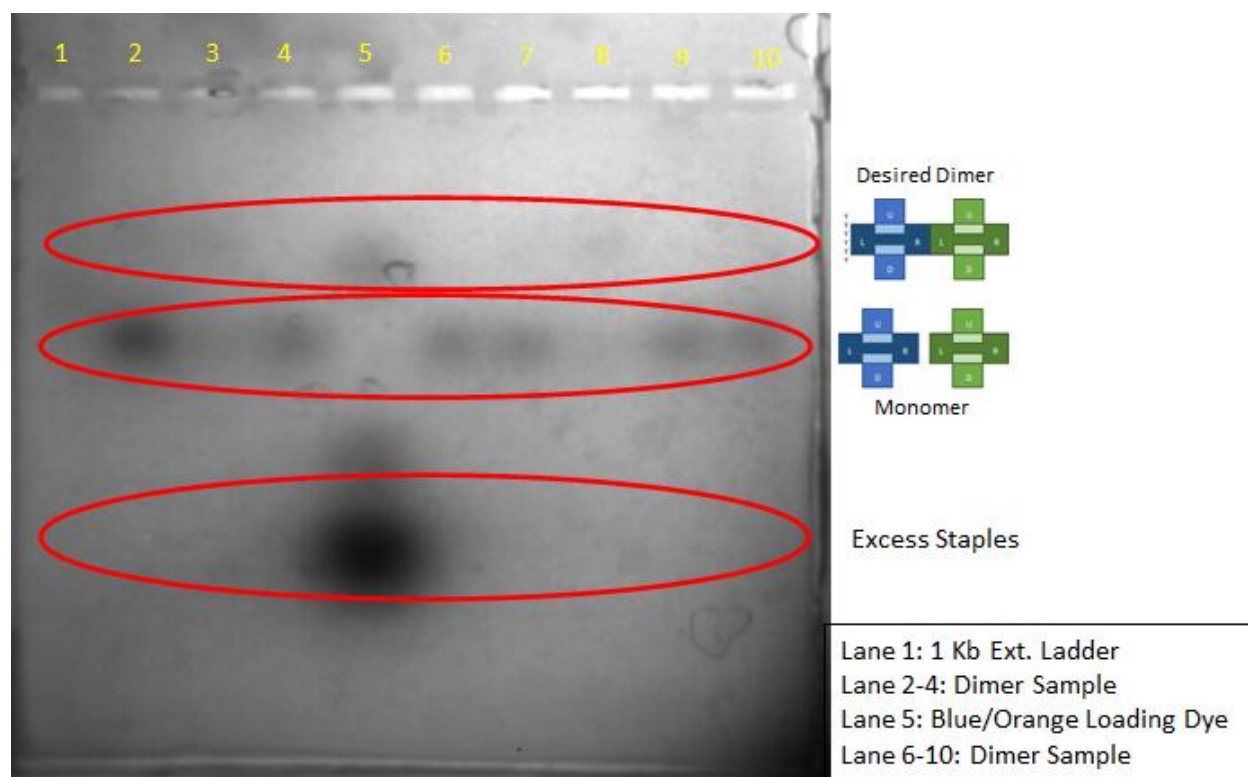


Figure 38. Shadowing Technique Using Dimer Sample. Gel image demonstrating the shadowing technique for a dimer sample. The monomer band, the middle red circle, is dark and distinguishable; however, the dimer band, the top red circle, is barely visible with only a few bands showing some darkness.

The final aspect of gel purification studied was UV-Table guided extraction. Since the shadowing technique lacked the definition needed for extraction in the dimer band, the staining technique was utilized instead. Prior to using the UV-table for extraction, the MiniBIS Pro UV Gel Doc was utilized to figure out where the desired bands were located. Since it was difficult to get accurate punctures from the gel via the MiniBIS Pro UV Gel Doc, the UV-Table was utilized to extract the desired bands from the gel. Figure 39 shows the extraction technique of cutting the lanes from the band and placing them on the UV-Table for specific band extraction

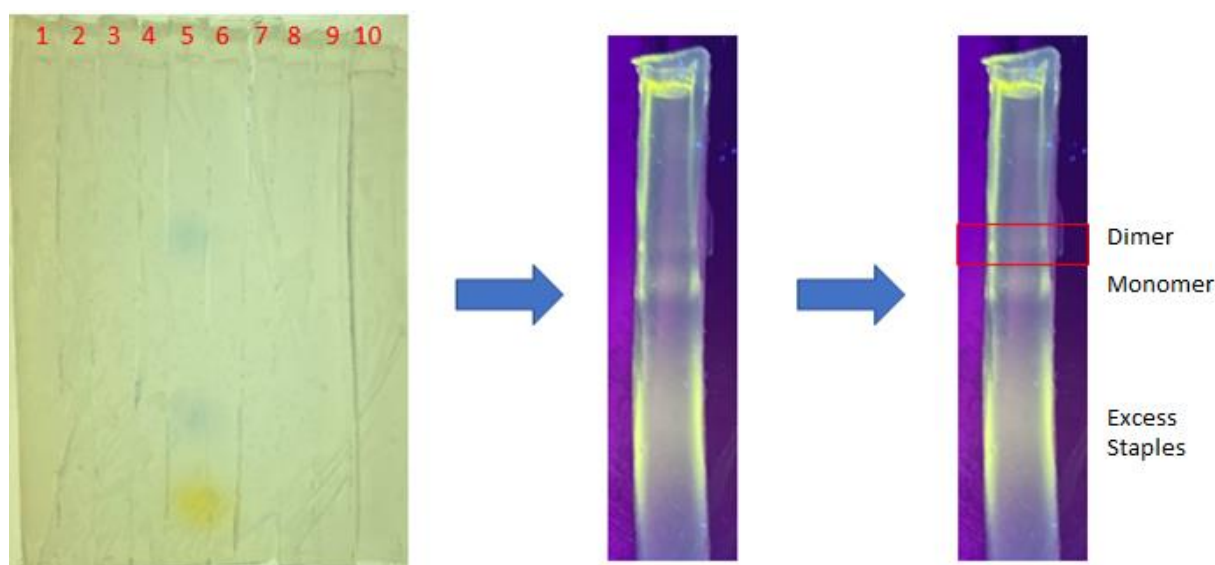


Figure 39. UV-Table Guided Extraction Using Dimer Product. Images of gel “lanes” at different stages in the extraction process. Taking the whole gel, sectioning apart each lane, and then extracting the desired dimer band. Lanes 1 – 4 and 6 – 10 contain dimer solution. Lane 5 contains Blue/Orange loading dye.

On Mica Assembly

When conducting the on-mica assembly, there was significant success production, deposition, and imaging of the 2-D arrays. The on- mica assembly technique was performed to determine whether 2-D arrays were properly forming in solution and depositing onto the mica substrate. An AFM image of the deposited assemblies shown in Figure 40. Figure 40 depicts multiple 2-D linear arrays which deposited onto the inserted mica substrate. However, the

agglomeration of the 2-D arrays caused issues when determining whether the 2-D arrays were properly formed. Since the mica substrate caused issues with the 2-D arrays agglomerating, glass was the next substrate used in experiments since it is the optimal final substrate for fluorescence imaging and spectral shift imaging.

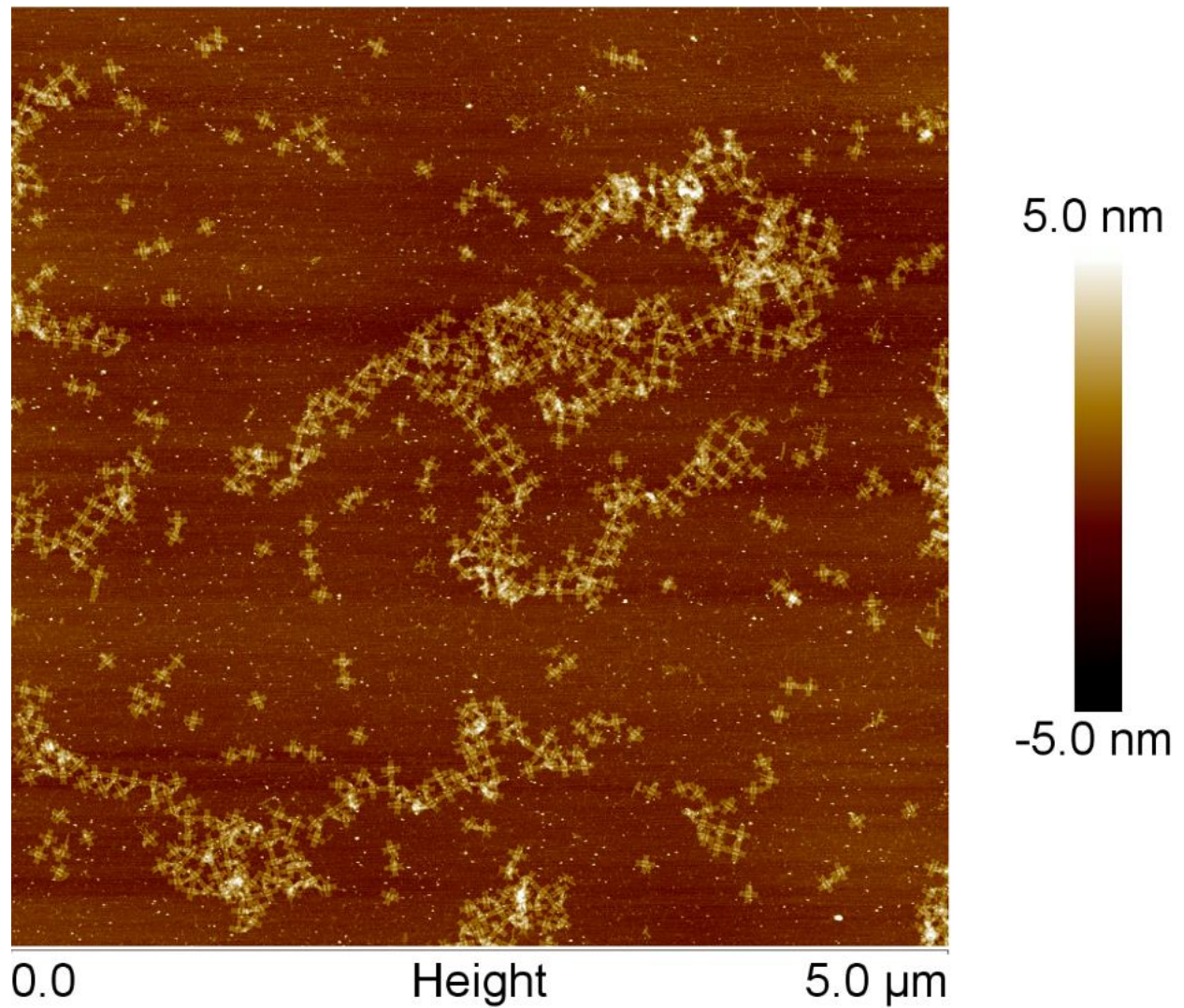


Figure 40. On Mica Assembly of 2-D Arrays

On Glass Assembly

When conducting the on-glass assembly, the deposition of 1-D arrays onto glass was relatively successful. The on-glass assembly technique allowed for non-agglomerated 1-D arrays to be found when imaged with the AFM. This is shown below in Figure 41.

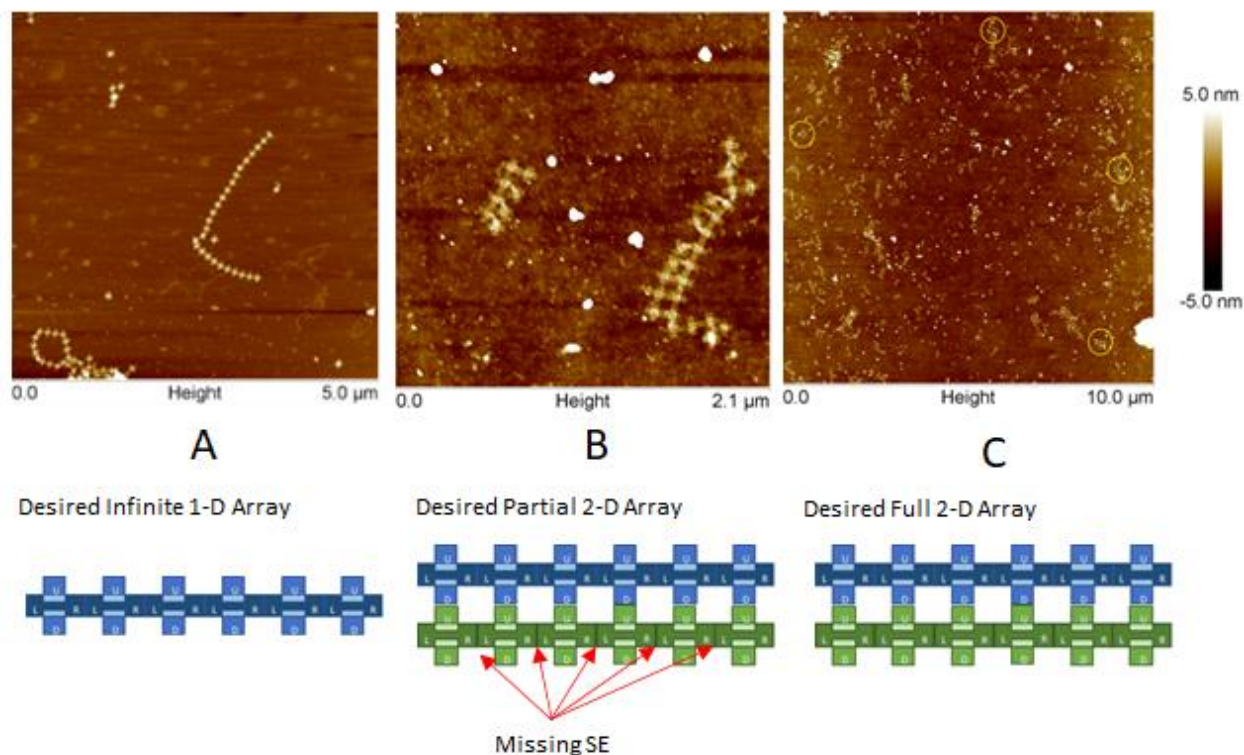


Figure 41. On Glass Assembly of 2-D Arrays. AFM images and associated representations for the on-glass assembly of 2-D arrays. Figure 41 A depicts the deposition of 1-D linear arrays onto glass. Figure 41 B depicts the addition of CO-3970 with the SE for CO-01 down arm and CO-3970 up arm to create partial 2-D arrays. Figure 41 C depicts the addition of SE for CO-3970 left and right arm to create full 2-D arrays.

Figure 41 A depicts 1-D linear arrays deposited on a glass substrate. Since the 1-D linear arrays are deposited via the in-solution method, 1-D linear arrays can be expected to deposit with higher array numbers per unit area. The ease in locating and imaging arrays proved that in-solution deposition on glass is a valid approach.

The next step of adding CO-3970 with only the up arms to CO-01 down arms was also found to be successful. Since the 1-D arrays were already on the cut glass, the cut glass with 1-D

arrays was placed into a solution of CO-3970 with just the up CO-3970 and down CO-01 SE. Figure 41 B shows the success of assembling the “partial” 2-D array. The 3970 sites are fully occupied, yet it is apparent that the 3970 components are not bound to each other. Since the partial 2-D arrays were assembled on glass correctly, the final step of adding the CO-3970 left and right SE was performed next.

Figure 41 C shows examples of the products of the final step, which entailed adding the CO-3970 left and right SE to the solution; however, the assembly was problematic. Finding the full 2-D array was difficult when imaging with the AFM and the amount of by-product forming from the excess of left and right SE created “pseudo” 1-D arrays of CO-3970. This is shown in Figure 41 C where 2-D arrays are forming, but an excess amount of incomplete product is still present. In view of this result, further purification methods for the product should be conducted in future work.

Dendrimer and Gold Nanoparticle

The synthesis of the prepared Dendron/DNA conjugates for attachment was successful. By following the four steps of attaching a thioester from SATP to primary amines on the dendrimer periphery, cleaving of dendrimers into dendrons with TCEP, reacting sulfo-SMCC with the primary amines on the DNA molecules, and conjugating of maleimide-activated DNA to the dendron core, Norton lab was able to successfully attach the modified CO-01 staple 175 to the dendron. Figure 42 shows that the conjugated DNA was attached to the dendron. This is visualized as an upper band forming in wells 2 and 3. The lower portion of the gel shows a band consisting of excess DNA.

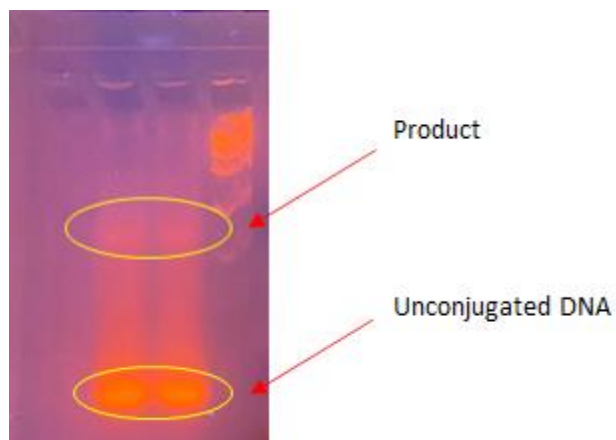


Figure 42. Gel with Refined Dendron to Conjugated DNA. Gel image demonstrating the success of conjugating the refined dendron to DNA.

Since these results are consistent with those in reference 20, it was concluded that the dendrons were successfully conjugated to the DNA. They were then purified, and thus the process of adding AuNP to the refined dendron with conjugated DNA was the next step. Although there were issues with the 40 nm AuNPs, the conjugates were successfully added to the refined dendron. This can be shown in the color shift of a light red to an even lighter shade of pink.

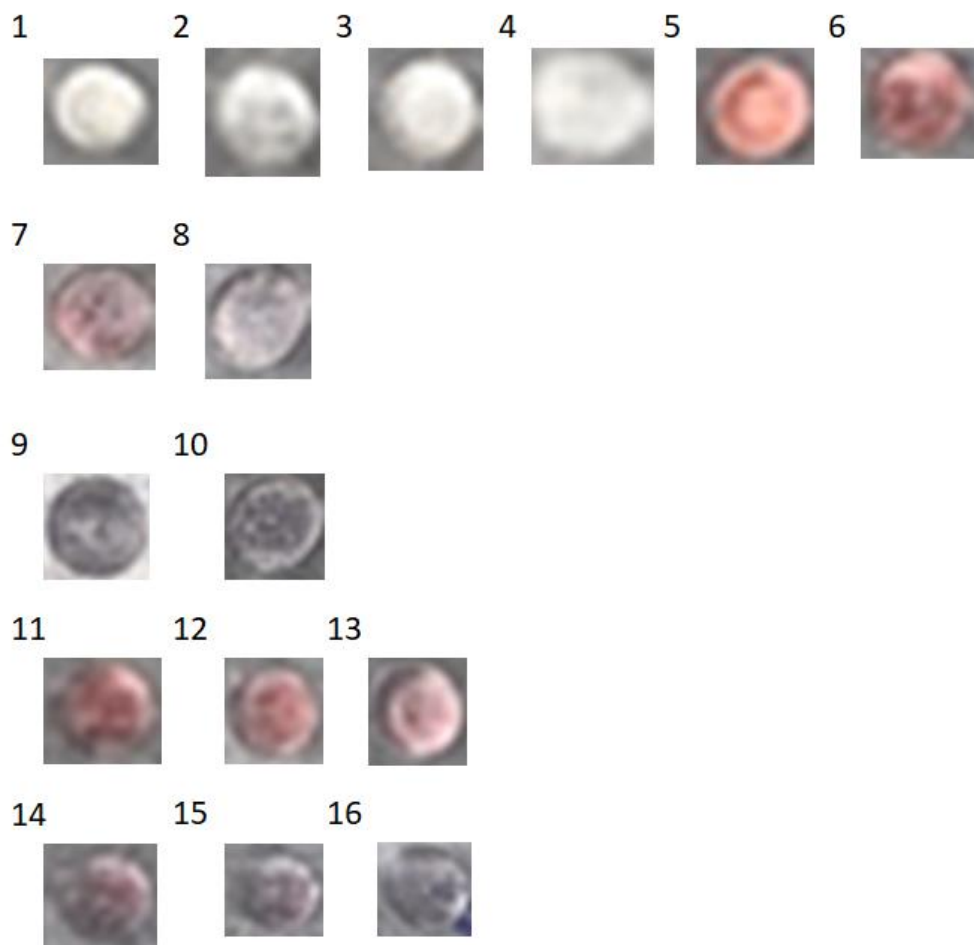


Figure 43. Shows the Color Shift of AuNP Solution when Adding Different Types of Salts and Refined Dendron to Conjugated DNA. Images presenting the color shift of the AuNP solution when adding $MgCl_2$ and refined dendron conjugated to DNA.

Table 4. Entry association with experiments in Figure 43.

Name	Number	Solution Volume	Observation	Interpretation
ddUVHOH	1	5 μ L	Colorless	Standard for colorless solution
0.5 X COB	2	5 μ L	Colorless	Just 0.5 X COB
0.025 M MgCl ₂	3	5 μ L	Colorless	Just 0.025 M MgCl ₂
Conjugate	4	5 μ L	Colorless	Just conjugate
AuNP	5	5 μ L	Red	Standard for red solution
AuNP	6	5 μ L	Red	The addition of conjugate to
Conjugate		5 μ L		AuNPs does not agglomerate the AuNPs
AuNP	7	5 μ L	Pink	The addition of conjugate and 0.5
Conjugate		5 μ L		X COB to AuNPs does not
0.5 X COB		5 μ L		agglomerate the AuNPs and solution turns pink
AuNP	8	5 μ L	Light Pink	The addition of conjugate and
Conjugate		5 μ L		excess 0.5 X COB to AuNPs does
0.5 X COB		10 μ L		not agglomerate the AuNPs and dilutes solution to light pink
AuNP	9	5 μ L	Dark Blue	The addition of conjugate and
Conjugate		5 μ L		0.025 M MgCl ₂ to AuNPs does
0.025 M MgCl ₂		5 μ L		agglomerate the AuNPs and solution turns dark blue
AuNP	10	5 μ L	Dark Blue	The addition of conjugate and
Conjugate		5 μ L		excess 0.025 M MgCl ₂ to AuNPs
0.025 M MgCl ₂		10 μ L		does agglomerate the AuNPs and solution turns dark blue
AuNP	11	5 μ L	Red	The addition of 2 μ L 0.5 X COB
0.5 X COB		2 μ L		does not agglomerate AuNPs and solution is red

AuNP 0.5 X COB	12	5 μ L 3 μ L	Red	The addition of 3 μ L 0.5 X COB does not agglomerate AuNPs and solution is red
AuNP 0.5 X COB	13	5 μ L 4 μ L	Pink	The addition of 4 μ L 0.5 X COB does not agglomerate AuNPs and solution dilutes to pink
AuNP 0.025 M MgCl ₂	14	5 μ L 2 μ L	Purple	The addition of 2 μ L 0.025 M MgCl ₂ does agglomerate AuNPs and solution is purple
AuNP 0.025 M MgCl ₂	15	5 μ L 3 μ L	Blue	The addition of 3 μ L 0.025 M MgCl ₂ does agglomerate AuNPs and solution is blue
AuNP 0.025 M MgCl ₂	16	5 μ L 4 μ L	Dark Blue	The addition of 4 μ L 0.025 M MgCl ₂ does agglomerate AuNPs and solution is dark blue

Figure 43 depicts the different types of experiments performed in order to determine the color shifts that occur when adding specific salts or conjugate to 40 nm AuNP. AuNPs by themselves are red when suspended in solution. When adding too much salt, the solution turns to a deep purple or blue color due to a shift in their plasmonic absorption of light and if the AuNPs fall out of solution/precipitate, the solution becomes colorless, with a black precipitate at the bottom of the droplet indicating that the AuNP are agglomerating. Conditions must be identified under which the AuNPs will not agglomerate because agglomeration would interfere with the synthesis required in the the plasmonic spectra shift experiments. So, by studying the effect of modifying the amount of salt and conjugate added, conditions were found in which the AuNPs stay suspended. This condition is indicated by the color of the solution turning from red into a lighter shade of red or pink. The final and future synthesis step would be to add the AuNP with the conjugate to the CO-01 in such a solution

CHAPTER 8

CONCLUSION

This work has shown that the synthesis of substrates for sensors using CO is possible, but highly problematic through SE modifications on the CO. AFM imaging depicts the synthesis of both 1-D and 2-D arrays confirming that many of the designs were successfully created even if the yield was lower than anticipated. The differences in concentration and incomplete products in the AFM images demonstrate that the gel purification and on glass deposition are capable of further improving the synthesis of the CO array components and substrates.

Even though yield is greatly reduced, the occurrence of some successful formation of 1-D and 2-D arrays provides a starting point for future platforms of sensors on 1-D and 2-D arrays. While the shadowing and staining with Sybr Gold techniques are still not fully perfected, isolating and purifying smaller products such as dimers can be done with great success.

When synthesizing the CO arrays, it is hypothesized that many CO products are formed but are sequestered into aggregations. This in turn renders it difficult to locate isolated individual CO arrays via AFM. Mica has been a consistent substrate for CO deposition since it is relatively flat and has a good affinity for DNA. However, when performing solution phase reactions with adsorption onto the surface of mica, we believe that CO arrays are formed, but are commonly found within aggregations, rendering them difficult to find via AFM imaging. Although surface deposition on mica provides a better population of arrays per unit area, glass is the final substrate for the modified CO arrays with sensors since optical imperfections in mica interferes with the imaging of sensors using fluorescence microscopy. Since surface deposition of the CO arrays on glass with short incubation times results in a low population of arrays per unit area, on glass deposition in solution was conducted with great success. Although there are

still aggregations appearing on glass, the technique of an in-solution deposition has presented a different technique for deposition onto glass.

Although sensors based on MBv2 and AuNPs were not specifically studied here, preliminary methods for experimentation were developed. With the fast scan AFM and the fluorescence microscope, recording the fluorescence for MBv2 can be monitored for super resolution. Although the AuNPs created issues with aggregation pre-experimentation, the synthesis of refined dendron to conjugated DNA was successful and is available for use in experiments directed toward characterizing plasmonic spectral shifts. We have made steps toward preparing useful AuNPs for future work. This would allow the measurement and studies of the AuNPs in plasmonic assemblies.

REFERENCES

1. Rothemund PWK. 2006. Folding DNA to create nanoscale shapes and patterns. *Nature*. 440(7082):297–302. <https://www.nature.com/articles/nature04586>.
doi:<https://doi.org/10.1038/nature04586>.
2. Liu W, Zhong H, Wang R, Seeman NC. 2010. Crystalline two-dimensional DNA-origami arrays. *Angewandte Chemie*. 123(1):278–281.
doi:<https://doi.org/10.1002/ange.201005911>.
3. Wu TC, Rahman M, Norton ML. 2014. From nonfinite to finite 1D arrays of origami tiles. *Accounts of Chemical Research*. 47(6):1750–1758.
doi:<https://doi.org/10.1021/ar400330y>.
4. Fan S, Wang D, Kenaan A, Cheng J, Cui D, Song J. 2019. Create nanoscale patterns with DNA origami. *Small*. 15(26):1805554. doi:<https://doi.org/10.1002/sml.201805554>.
5. Marchi AN, Saaem I, Vogen BN, Brown S, LaBean TH. 2014. Toward larger DNA origami. *Nano Letters*. 14(10):5740–5747. doi:<https://doi.org/10.1021/nl502626s>.
6. Ariga K, Mori T, Nakanishi W, Hill JP. 2017. Solid surface vs. liquid surface: nanoarchitectonics, molecular machines, and DNA origami. *Physical Chemistry Chemical Physics*. 19(35):23658–23676. doi:<https://doi.org/10.1039/c7cp02280h>.
7. Endo M, Sugiyama H. 2018. DNA origami nanomachines. *Molecules*. 23(7):1766.
doi:<https://doi.org/10.3390/molecules23071766>.
8. Seeman NC. 2010. Nanomaterials based on DNA. *Annual Review of Biochemistry*. 79(1):65–87. doi:<https://doi.org/10.1146/annurev-biochem-060308-102244>.

9. Liu X, Farmerie W, Schuster S, Tan W. 2000. Molecular beacons for DNA biosensors with micrometer to submicrometer dimensions. *Analytical Biochemistry*. 283(1):56–63. doi:<https://doi.org/10.1006/abio.2000.4656>.
10. Watson J. 2004. Definitions and analysis of DNA Holliday junction geometry. *Nucleic Acids Research*. 32(10):3017–3027. doi:<https://doi.org/10.1093/nar/gkh631>.
11. Potaman V, Sinden R. 2000. In *Madame Curie Bioscience Database*:1–14.
12. M13mp18 Single-stranded DNA | NEB. www.neb.com. [accessed 2023 Apr 7].
<https://www.neb.com/products/n4040-m13mp18-single-stranded-dna#Product%20Information>.
13. Weber P, Ohlendorf D, Wendoloski J, Salemme F. 1989. Structural origins of high-affinity biotin binding to streptavidin. *Science*. 243(4887):85–88. doi:<https://doi.org/10.1126/science.2911722>.
14. Reznik GO, Vajda S, Smith CL, Cantor CR, Sano T. 1996. Streptavidins with intersubunit crosslinks have enhanced stability. *Nature Biotechnology*. 14(8):1007–1011. doi:<https://doi.org/10.1038/nbt0896-1007>.
15. Sacca B, Niemeyer CM. 2012. ChemInform abstract: DNA origami: the art of folding DNA. *ChemInform*. 43(14):no-no. doi:<https://doi.org/10.1002/chin.201214263>.
16. Murphy DB, Davidson MW. 2013. *Fundamentals of light microscopy and electronic imaging*. Hoboken, N.J.: Wiley-Blackwell.
17. McLeod E, Ozcan A. 2014. Nano-imaging enabled via self-assembly. *Nano Today*. 9(5):560–573. doi:<https://doi.org/10.1016/j.nantod.2014.08.005>.
18. Jockusch S, Martí AA, Turro NJ, Li Z, Li X, Ju J, Stevens N, Akins DL. 2006. Spectroscopic investigation of a FRET molecular beacon containing two fluorophores for

- probing DNA/RNA sequences†. *Photochemical & Photobiological Sciences*. 5(5):493–498. doi:<https://doi.org/10.1039/b600213g>.
19. Tan W, et al. et al. 2009. ChemInform abstract: molecular engineering of DNA: molecular beacons. *ChemInform*. 40(14). doi:<https://doi.org/10.1002/chin.200914273>.
 20. Wikipedia Contributors. 2019 Nov 19. Förster resonance energy transfer. Wikipedia. https://en.wikipedia.org/wiki/F%C3%B6rster_resonance_energy_transfer#/media/File:FR_ET_Jablonski_diagram.svg.
 21. CytoViva | Enhanced Darkfield Hyperspectral Microscope | Products. CytoViva, Inc. [accessed 2023 Apr 7]. <https://www.cytoviva.com/products/3d-enhanced-darkfield-imaging>.
 22. Warner CN, Hunter ZD, Carte DD, Skidmore TJ, Vint ES, Day BS. 2020. Structure and function analysis of DNA monolayers created from self-assembling DNA–dendron conjugates. *Langmuir*. 36(19):5428–5434. doi:<https://doi.org/10.1021/acs.langmuir.0c00340>.
 23. Zanchet D, Micheel CM, Parak WJ, Gerion D, Alivisatos AP. 2000. Electrophoretic isolation of discrete Au nanocrystal/DNA conjugates. *Nano Letters*. 1(1):32–35. doi:<https://doi.org/10.1021/nl005508e>.
 24. Tomalia DA. 2005. The dendritic state. *Materials Today*. 8(3):34–46. doi:[https://doi.org/10.1016/s1369-7021\(05\)00746-7](https://doi.org/10.1016/s1369-7021(05)00746-7). <https://www.sciencedirect.com/science/article/pii/S1369702105007467>.
 25. Juluri BK, Zheng YB, Ahmed D, Jensen L, Huang TJ. 2008. Effects of geometry and composition on charge-induced plasmonic shifts in gold nanoparticles. *The Journal of Physical Chemistry C*. 112(19):7309–7317. doi:<https://doi.org/10.1021/jp077346h>.

26. Ijäs H, Nummelin S, Shen B, Kostianen M, Linko V. 2018. Dynamic DNA origami devices: from strand-displacement reactions to external-stimuli responsive systems. *International Journal of Molecular Sciences*. 19(7):2114. doi:<https://doi.org/10.3390/ijms19072114>.
27. Kuzuya A, Komiyama M. 2010. DNA origami: fold, stick, and beyond. *Nanoscale*. 2(3):310–322. doi:<https://doi.org/10.1039/b9nr00246d>. [accessed 2020 Feb 9]. <https://pubs.rsc.org/en/content/articlelanding/2010/nr/b9nr00246d#>
28. Lukhmanov E. 2022. Personal Communication.
29. Day BS, Fiegand LR, Vint ES, Shen W, Morris JR, Norton ML. 2011. Thiolated dendrimers as multi-point binding headgroups for DNA immobilization on gold. *Langmuir*. 27(20):12434–12442. doi:<https://doi.org/10.1021/la202444s>.

APPENDIX A: OFFICE OF RESEARCH INTEGRITY APPROVAL LETTER



Office of Research Integrity

November 9, 2022

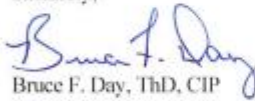
Nathan Shin
528 Hal Greer Blvd.
Huntington, WV 25703

Dear Nathan:

This letter is in response to the submitted thesis abstract entitled "*Sequential Assembly of 1-D and 2-D Origami Arrays.*" After assessing the abstract, it has been deemed not to be human subject research and therefore exempt from oversight of the Marshall University Institutional Review Board (IRB). The Code of Federal Regulations (45CFR46) has set forth the criteria utilized in making t/his determination. Since the information in this study does not involve human subjects as defined in the above referenced instruction, it is not considered human subject research. If there are any changes to the abstract, you provided then you would need to resubmit that information to the Office of Research Integrity for review and a determination.

I appreciate your willingness to submit the abstract for determination. Please feel free to contact the Office of Research Integrity if you have any questions regarding future protocols that may require IRB review.

Sincerely,



Bruce F. Day, ThD, CIP
Director

WE ARE... MARSHALL.

One John Marshall Drive • Huntington, West Virginia 25755 • Tel 304/696-4303
A State University of West Virginia • An Affirmative Action/Equal Opportunity Employer

APPENDIX B: LIST OF ABBREVIATIONS

AFM Atomic Force Microscopy

AuNP gold nanoparticle

CO Cross Origami

COB cross origami buffer

DI deionized

DMSO dimethyl sulfoxide

DNA deoxyribonucleic acid

EtBr ethidium bromide

FRET fluorescence resonance energy transfer

G2 PAMAM dendrimer generation 2 polyamidoamine dendrimer

Hz hertz

MBv2 molecular beacon version 2

MM8 AFM multimode 8 atomic force microscope

MgCl₂ Magnesium Chloride

NMWL nominal molecular weight limit

PBS phosphate-buffered saline

PCR polymerase chain reaction

SA Streptavidin

SATP N-succinimidyl-S-acetylthiopropionate

SE sticky ends

SSMCC sulfosuccinimidyl-4-(N-maleimidomethyl) cyclohexane-1-carboxylate

T terminator

TAE tris-acetate-EDTA

TCEP tris(2-carboxyethyl)phosphine hydrochloride

TLC thin layer chromatography

UV ultraviolet

V volts

cm centimeters

ddUV double distilled UV treated

dsDNA double stranded DNA

mL milliliters

mM millimolar

nM nanomolar

ng nanograms

nm nanometers

rpm revolutions per minute

ssDNA single stranded DNA

μ M micromolar

μ m micrometers

APPENDIX C: FIGURE PERMISSION FOR SEEMAN'S CO-01 DESIGN FIGURE 9

JOHN WILEY AND SONS LICENSE TERMS AND CONDITIONS

Nov 07, 2022

This Agreement between Marshall University -- Nathan Shin ("You") and John Wiley and Sons ("John Wiley and Sons") consists of your license details and the terms and conditions provided by John Wiley and Sons and Copyright Clearance Center.

License Number	5423801099168
License date	Nov 07, 2022
Licensed Content Publisher	John Wiley and Sons
Licensed Content Publication	Angewandte Chemie International Edition
Licensed Content Title	Crystalline Two-Dimensional DNA-Origami Arrays
Licensed Content Author	Wenyan Liu, Hong Zhong, Risheng Wang, et al
Licensed Content Date	Nov 4, 2010
Licensed Content Volume	50
Licensed Content Issue	1
Licensed Content Pages	4
Type of use	Dissertation/Thesis
Requestor type	University/Academic
Format	Print and electronic
Portion	Figure/table
Number of figures/tables	1
Will you be translating?	No
Title	SEQUENTIAL ASSEMBLY OF 1-D AND 2-D ORIGAMI ARRAYS
Institution name	Marshall University
Expected presentation date	Dec 2022
Portions	Figure S1
Requestor Location	Marshall University 2 Chatham Rd. CHARLESTON, WV 25304 United States Attn: Marshall University
Publisher Tax ID	EU826007151
Total	0.00 USD

APPENDIX D: S1 AND S6

Table 5. S1 Contents

S1	[i]	Volume	[f]
Binder-crosslinker staples #1	5000 nM	30 μ L	500 nM
LRA open 4, 9, 10, 16 #2	5000 nM	30 μ L	500 nM
LRB #3	5000 nM	30 μ L	500 nM
LRC #4	5000 nM	30 μ L	500 nM
LRD open 74 and 81 #5	5000 nM	30 μ L	500 nM
UDA open 99, 100, 104, 105 #6	5000 nM	30 μ L	500 nM
UDB #9	5000 nM	30 μ L	500 nM
UDC #12	5000 nM	30 μ L	500 nM
UDD no 175, 175, 176 #13	5000 nM	30 μ L	500 nM
UDA 99, 100, 104.105 Only #7	5000 nM	30 μ L	500 nM
TOTAL VOLUME		300 μ L	

Table 6. S6 Contents

S6	[i]	Volume	[f]
CO-01 4,10, 16 Only #8	5000 nM	60 μ L	1000 nM
CO-01 99 Biotin and 105 Biotin	5000 nM	60 μ L	1000 nM
CO-01 174, 175, 176 Only #14	5000 nM	60 μ L	1000 nM
CO-01 74 and 81 Only #10	5000 nM	60 μ L	1000 nM
HOH		60 μ L	
TOTAL VOLUME		300 μ L	

APPENDIX E: MONOMER COUNT FOR TABLE 3

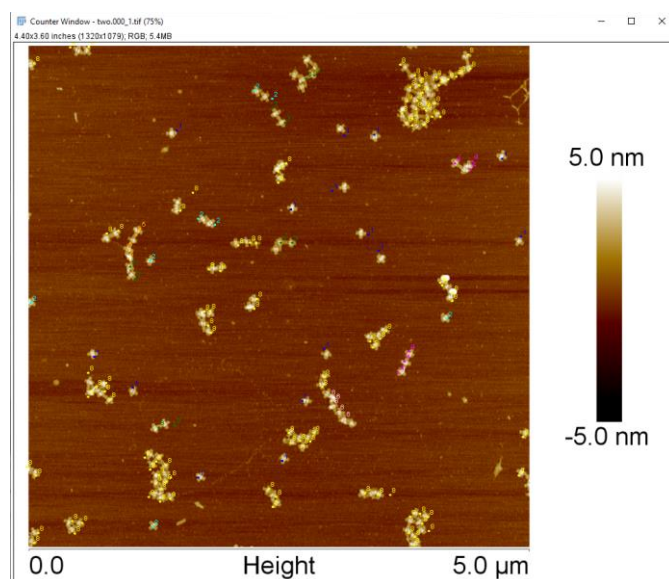


Figure 44 A. 4:1 CO-01 to CO-3970. Blue is monomer with SA, cyan is monomer with no SA, green is dimer, magenta is trimer, orange is 4-mer, light pink is 5-mer, pink is 6-mer, and yellow is unidentifiable. There are 11 blue, 2 cyan, 2 green, 3 magenta, 20 orange, 0 light pink, 0 pink, and 18 yellow.

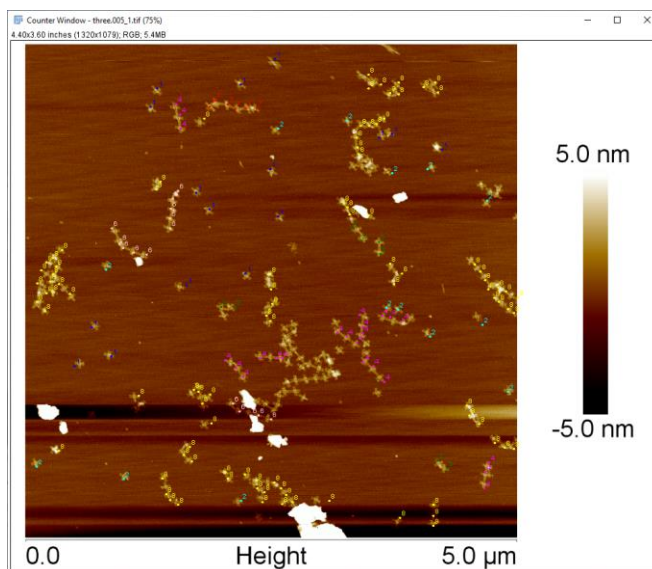


Figure 44 B. 2:1 CO-01 to CO-3970. Blue is monomer with SA, cyan is monomer with no SA, green is dimer, magenta is trimer, orange is 4-mer, light pink is 5-mer, pink is 6-mer, and yellow is unidentifiable. There are 15 blue, 8 cyan, 10 green, 6 magenta, 4 orange, 5 light pink, 0 pink, and 113 yellow.

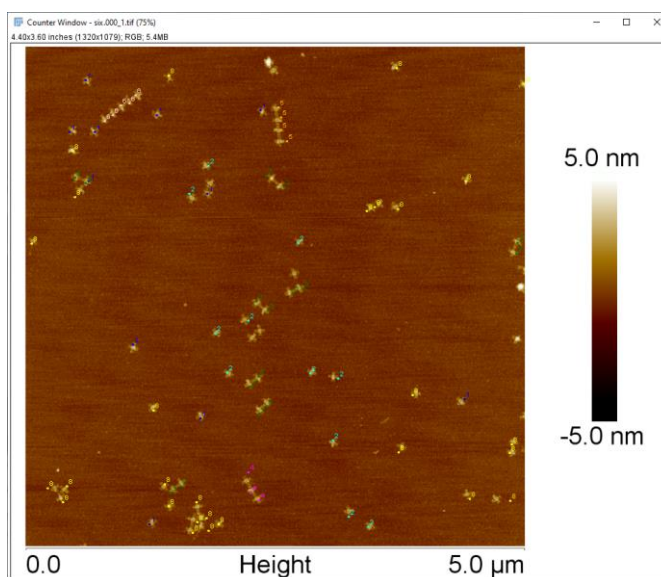


Figure 44 C. 1:1 CO-01 to CO-3970. Blue is monomer with SA, cyan is monomer with no SA, green is dimer, magenta is trimer, orange is 4-mer, light pink is 5-mer, pink is 6-mer, and yellow is unidentifiable. There are 11 blue, 14 cyan, 8 green, 24 magenta, 0 orange, 15 light pink, 6 pink, and 85 yellow.

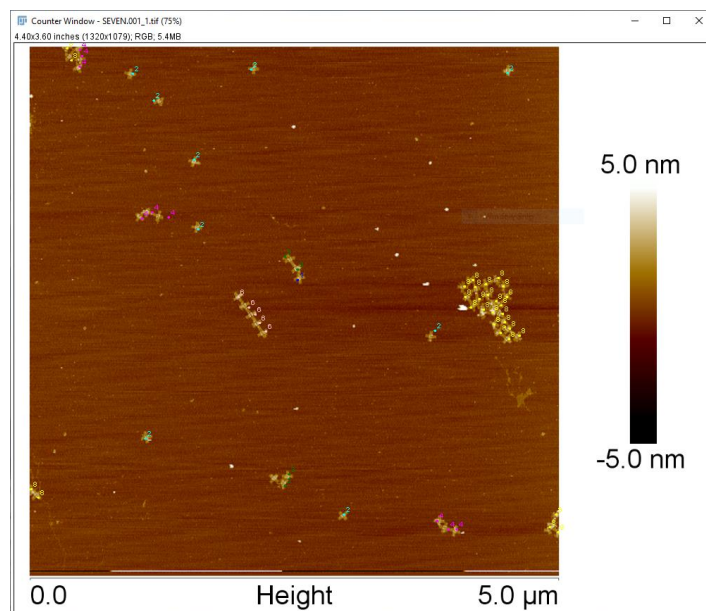


Figure 44 D. 1:2 CO-01 to CO-3970. Blue is monomer with SA, cyan is monomer with no SA, green is dimer, magenta is trimer, orange is 4-mer, light pink is 5-mer, pink is 6-mer, and yellow is unidentifiable. There are 11 blue, 11 cyan, 16 green, 3 magenta, 4 orange, 5 light pink, 0 pink, and 29 yellow.

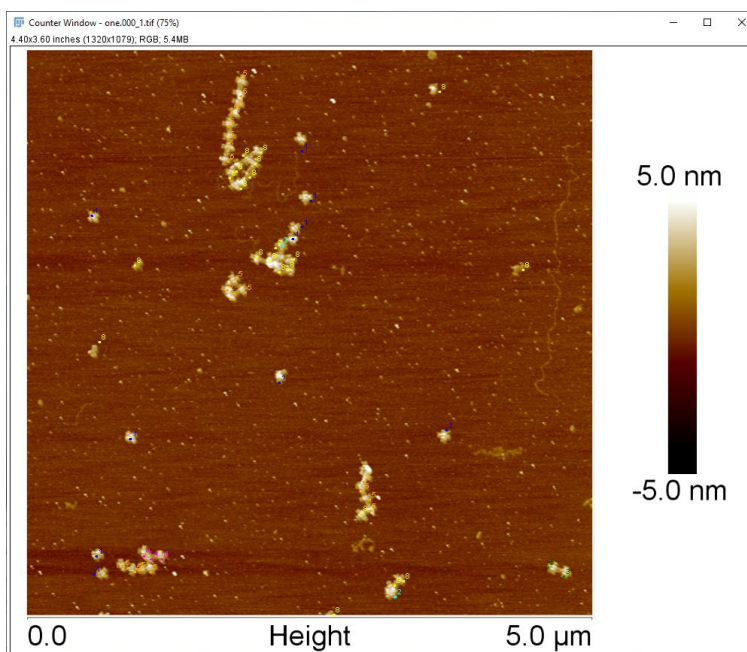


Figure 44 E. 1:4 CO-01 to CO-3970. Blue is monomer with SA, cyan is monomer with no SA, green is dimer, magenta is trimer, orange is 4-mer, light pink is 5-mer, pink is 6-mer, and yellow is unidentifiable. There are 1 blue, 9 cyan, 2 green, 9 magenta, 0 orange, 5 light pink, 0 pink, and 29 yellow.